FEATURE ARTICLE

Check for updates

Exploring the multifaceted applications of antimony(III/V) corrole complexes†

Arup Tarai, [ID] *[abc] Tanmoy Pain,[bc] Subhajit Kar,‡[bc] Rwiddhi Chakraborty‡[bc] and Sanjib Kar [ID] *[bc]

Tetrapyrrolic macrocycles coordinated to redox-active main-group elements, particularly from groups 14 and 15, have emerged as efficient photocatalysts for substrate oxidation under ambient conditions. Among group 15 elements, antimony commonly adopts +III and +V oxidation states and forms stable high-valent complexes with porphyrinoid ligands such as corroles, which readily accommodate diverse axial ligands (*e.g.*, O-, N-, and S-donors). Antimony corrole complexes exhibit considerable promise across diverse fields, including catalysis, biomedicine, and advanced dielectric and optoelectronic applications. The oxidation state of antimony plays a crucial role in modulating key reactivities such as photo- and electrochemical C–H bond activation, hydrogen evolution, and triplet-to-singlet oxygen conversion. The generation of singlet oxygen, a highly reactive species, underpins their use in catalytic oxidation and photodynamic therapy. Additionally, the tunable electronic structures of these complexes render them attractive candidates for next-generation optoelectronic and dielectric materials. This review highlights the multifunctionality of antimony corroles, encouraging further exploration of structural modifications to expand their application landscape.

[a] Department of Chemistry, Mahila Mahavidyalaya (MMV), Banaras Hindu University (BHU), Varanasi 221005, India. E-mail: aruptarai@bhu.ac.in, aruptarai@gmail.com
[b] School of Chemical Sciences, National Institute of Science Education and Research (NISER), Bhubaneswar−752050, India. E-mail: sanjib@niser.ac.in
[c] Homi Bhabha National Institute, Mumbai 400094, India
† Dedicated to Professor Mangalampalli Ravikanth on the occasion of his 60th birthday.
‡ Both authors contributed equally to this work.

Arup Tarai is currently working as an Assistant Professor in Chemistry at Mahila Mahavidyalaya (MMV), Banaras Hindu University (BHU), India. His academic journey in chemistry began with a BSc from Midnapore College, followed by MSc from IIT Kharagpur. He earned his PhD in Chemistry from IIT Guwahati in 2018, under the supervision of Prof. Jubaraj B. Baruah. Following his PhD, Dr Tarai pursued postdoctoral research at Shenzhen University

Arup Tarai

(from July 2019 to June 2021), China with Prof. Zhigang Yang and Prof. Junle Qu. Subsequently, he joined Prof. Sanjib Kar's research group at the School of Chemical Sciences, NISER Bhubaneswar as a postdoctoral researcher (from April 2022 to Oct. 2023), where he focused on the synthesis and modification of various corroles/metallo-corroles. Currently, he is working on designing main group element based luminescent materials for optoelectronic applications.

Tanmoy Pain is currently working as a Postdoctoral Fellow (NSTC Fellow) in Inorganic Chemistry at the Institute of Chemistry, Academia Sinica, Taiwan, under the supervision of Prof. Chen Hsiung Hung. He received his BSc in Chemistry from The University of Burdwan, India, in 2013, and his MSc in Inorganic Chemistry from Guru Ghasidas Vishwavidyalaya (Central University), India, in 2016. Dr Pain earned his PhD in Inorganic Chemistry in 2024 from the

Tanmoy Pain

National Institute of Science Education and Research (NISER), Bhubaneswar, India, under the guidance of Prof. Sanjib Kar. Following his PhD, Dr Pain worked as a Research Associate-I at NISER Bhubaneswar for five months before joining Academia Sinica. His research interests centre on the design, modification, and study of tetrapyrrolic macrocycles, with a focus on their applications in electrochemistry, photophysics, and functional materials.

1. Introduction

1.1. General features of antimony(III/V)-corrole complexes

Corroles are aromatic, tetrapyrrolic macrocyclic ligands structurally related to porphyrins but they have a contracted framework due to the absence of one *meso*-carbon, resulting in a 23-atom macrocycle that differs from porphyrins both topologically and electronically.[1–5] Free-base (FB) porphyrins are diprotonic ligands, whereas FB corroles are inherently triprotonic.[6,7] Due to their increased acidity and greater electron richness, corroles act as trianionic ligands upon metal coordination, in contrast to the dianionic character of porphyrins. This unique combination of properties enables corroles to stabilize metal ions in higher oxidation states than porphyrins.[8–10] First described by Johnson and Kay in 1965,[11] corrole chemistry remained underdeveloped for several decades due to synthetic challenges. The emergence of reliable synthetic methodologies in the late 1990s, however, significantly revitalized interest in corrole-based coordination compounds.[12,13] Corroles can coordinate a wide range of metal ions across multiple oxidation states.[14,15] In particular, main-group metal complexes, such as those incorporating group 15 elements like antimony, exhibit oxidation-state-dependent behavior, typically forming $Sb(III)$ or $Sb(V)$ complexes under different reaction conditions.[16] Corroles readily form air-stable $Sb(V)$ complexes, including both oxo and halide derivatives, characterized by well-defined coordination geometries and reversible redox behavior—features that stand in contrast to those of metal–porphyrin systems, which often display reduced redox accessibility and limited coordination flexibility for stabilizing high-valent species.[17–19] Metallocorroles, unlike their porphyrin analogues, often undergo three successive macrocycle-centered oxidations, affording broader redox windows and greater tunability of electronic structure.[19,20] These properties are particularly advantageous in the design of molecular catalysts and photosensitizers, where precise control over redox potentials and the stabilization of reactive intermediates are critical. In the case of antimony corroles, the accessibility of $Sb(III)/Sb(V)$ redox couples, moderate axial ligand exchange, and stable redox profiles support their potential use in multielectron photoredox processes. Furthermore, antimony corroles exhibit enhanced photostability and electronic versatility, facilitating catalytic transformations under mild conditions that are often challenging for porphyrin-based systems. Compared to other main-group metallocorroles—such as those of gallium,[21] tin,[22] bismuth,[23] or phosphorus[24]—antimony complexes offer a favorable combination of multivalency, axial lability, and photoactivity, making them attractive candidates for applications in redox-active materials and light-driven catalysis.[25,26] As

Subhajit Kar

Subhajit Kar received his BSc in Chemistry from The University of Burdwan in 2019 and his MSc from the Indian Institute of Technology (Indian School of Mines), Dhanbad, in 2021. He is currently pursuing a PhD in inorganic chemistry at the National Institute of Science Education and Research (NISER), Bhubaneswar, India, under the supervision of Prof. Sanjib Kar. His research focuses on the synthesis, structural characterisation, and advanced spectroscopic studies of corrole-metal complexes, with particular interest in their electronic structures and functional properties.

Rwiddhi Chakraborty

Rwiddhi Chakraborty obtained her BSc in Chemistry from the University of Calcutta in 2020, followed by an MSc in Chemistry from the University of Hyderabad in 2022. She is currently a doctoral researcher in inorganic chemistry at the National Institute of Science Education and Research (NISER), Bhubaneswar, India, under the supervision of Prof. Sanjib Kar. Her research centers on the design and functional modification of tetrapyrrolic macrocycles, including both free-base and metallated derivatives, with a particular emphasis on their electrochemical properties and potential applications.

Sanjib Kar

Sanjib Kar received his BSc and MSc degrees in chemistry from the University of Burdwan and the University of Kalyani, respectively, in West Bengal, India. He obtained his PhD in inorganic chemistry from the Indian Institute of Technology Bombay in December 2005, under the supervision of Professor G. K. Lahiri. In April 2006, he joined the research group of Professor Yoshinori Naruta at Kyushu University, Japan, as a JSPS postdoctoral fellow. In 2009, he began his independent academic career as an Assistant Professor at the School of Chemical Sciences, National Institute of Science Education and Research (NISER), Bhubaneswar, where he was promoted to Professor in 2023. His research interests focus on the design, synthesis, and functional applications of porphyrinoid and metalloporphyrinoid-based systems.
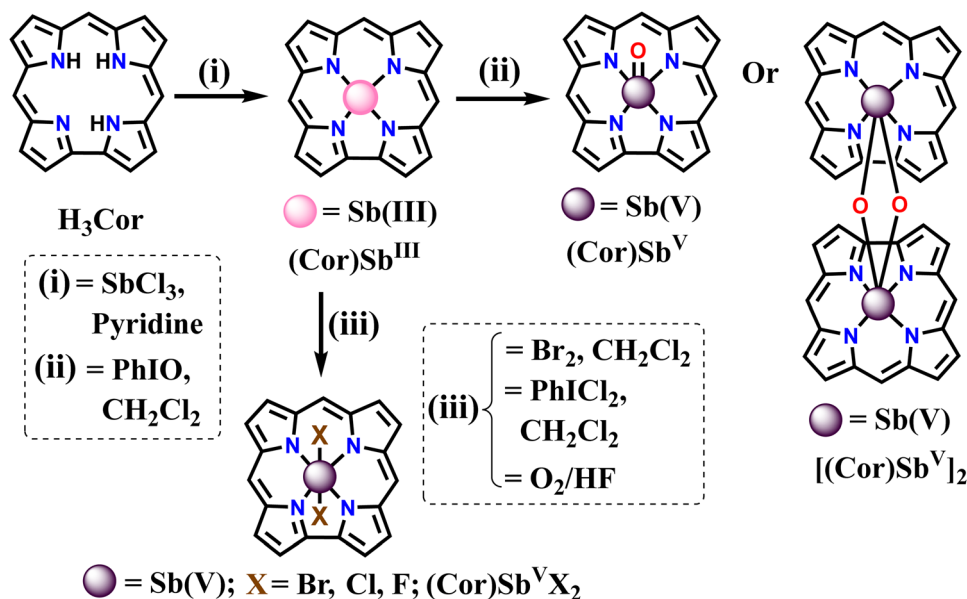
Fig. 1 Schematic presentation of the synthesis of antimony(III)-corrole, halogenated antimony(V)-corrole, (oxo)antimony(V)-corrole, and dimeric antimony(V)-corrole from their respective free base corroles.

illustrated in Fig. 1, free-base (FB) corroles react with SbCl$_3$ in the presence of pyridine to yield Sb(III)–corrole complexes. These can be further oxidized to Sb(v) derivatives – such as halogenated, oxo-, and dimeric Sb(v)-corroles – under suitable oxidative conditions. Kadish and co-workers reported a stepwise oxidation of Sb(III)-octaethylcorrole to Sb(IV) and ultimately to Sb(v), with each one-electron oxidation occurring at the metal center *via* a transient Sb(IV) intermediate.[19] Not only with metal ions, corroles readily

interact with a variety of anions, forming stable anionic adducts through strong electrostatic and coordination interactions.[27–30]

Gross and co-workers synthesized and comprehensively characterized three antimony–corrole complexes: antimony (III)–corrole **{(Cor)Sb^{III}-1}**, (oxo)antimony(v)-corrole **{(Cor)Sb^{V}-2}**, and *trans*-difluoroantimony(v)-corrole **{(Cor)Sb^{V}-3}** using a range of spectroscopic and crystallographic techniques.[31] These complexes were derived from the FB ligand 5,10,15-tris(pentafluorophenyl)corrole.
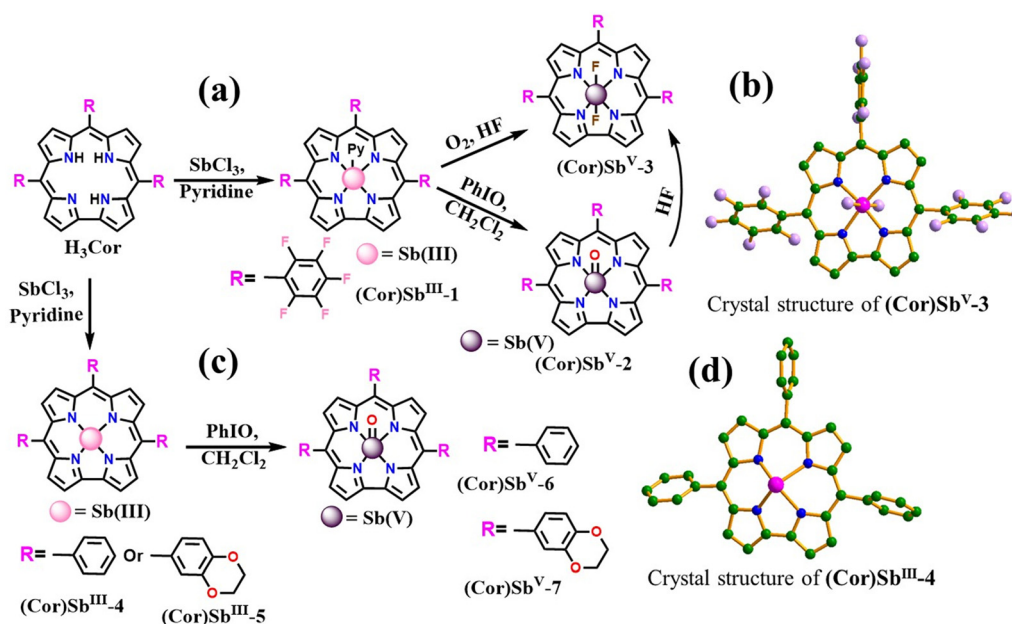

Fig. 2 (a) and (c) Molecular structure of different FB corroles, antimony(III)-corrole **{(Cor)Sb^{III}-1}**, (oxo)antimony(v)-corrole **{(Cor)Sb^{V}-2}** and *trans*-difluoroantimony(v)-corrole **{(Cor)Sb^{V}-3}**, and (b and d) crystal structures of **(Cor)Sb^{V}-3**[31] and **(Cor)Sb^{III}-4**.[34] Adapted from ref. 31 with permission from the ChemComm. © 2006 American Chemical Society. Adapted from ref. 34 with permission from Elsevier. © 2020 Elsevier.

In {(Cor)Sb^III-1}, a penta-coordinate geometry was observed, with pyridine occupying the axial site. Single-crystal X-ray diffraction confirmed the solid-state structures of all three complexes. Notably, while {(Cor)Sb^III-1} and {(Cor)Sb^V-2} adopted dome-shaped corrole conformations, {(Cor)Sb^V-3} exhibited a near-planar macrocyclic geometry with the metal center residing in the plane of the ligand (Fig. 2a and b). All three complexes were evaluated as photocatalysts for the aerobic oxidation of thioanisole under visible light, with ethanol identified as the optimal solvent. Under similar conditions, selective oxidation of allylic and benzylic C–H bonds also proceeded efficiently, affording the corresponding hydroperoxides. The observed catalytic performance followed the order: {(Cor)Sb^III-1} < {(Cor)Sb^V-2} < {(Cor)Sb^V-3}. Mechanistic investigations indicated that singlet oxygen generated upon photoirradiation served as the sole reactive oxidant in these transformations. To elucidate the superior singlet oxygen generation efficiency of (Cor)Sb^V-3 relative to (Cor)Sb^III-1 and (Cor)Sb^V-2, Gross and co-workers performed detailed time-resolved electron paramagnetic resonance (EPR) and optical spectroscopic studies.[32] These investigations revealed that the planar geometry of (Cor)Sb^V-3 facilitates enhanced d-π electron coupling between the antimony(V) center and the corrole ligand, in contrast to the dome-shaped geometries of the other two complexes. This stronger electronic interaction significantly boosts the efficiency of singlet oxygen generation, thereby improving the photocatalytic activity of (Cor)Sb^V-3.

Further photophysical characterization was carried out using femtosecond broadband fluorescence up-conversion and femtosecond Vis-pump/Vis-probe transient absorption spectroscopy.[33] These ultrafast measurements confirmed that (Cor)Sb^V-3 exhibits pronounced spin–orbit coupling and an efficient intersystem crossing pathway, consistent with its high singlet oxygen quantum yield.

Kar et al. synthesized and characterized two corroles with different meso-carbon substitutions: 5,10,15-triphenylcorrole and 5,10,15-tris[3,4-(1,4-dioxan)phenyl]corrole, along with their corresponding antimony(III) complexes. These antimony(III) corroles, (Cor)Sb^III-4 and (Cor)Sb^III-5, were further oxidized to the corresponding (oxo)antimony(V) corroles, (Cor)Sb^V-6 and (Cor)Sb^V-7, in the presence of the oxidizing agent iodosobenzene (Fig. 2c), following a reported protocol by Gross et al.[31] The crystal structure of (Cor)Sb^III-4 revealed that it is a dome shaped corrole complex, deviating from the corrole plane by ~0.963–0.966 Å (Fig. 2d).[34] All four complexes; (Cor)Sb^III-4, (Cor)Sb^III-5, (Cor)Sb^V-6 and (Cor)Sb^V-7 were confirmed to be diamagnetic based on ¹H NMR spectroscopy, as all their chemical shifts were within the expected normal range. The (Cor)Sb^III-4 and (Cor)Sb^III-5 displayed split Soret bands in the range of 440–462 nm, while (Cor)Sb^V-6 and (Cor)Sb^V-7 exhibited a single Soret band in the range of 408–413 nm. All four complexes exhibited emission peaks at 630–650 nm and a shoulder at 690–710 nm in CH₂Cl₂.[34] This finding indicates that the oxidation state and coordination environment significantly influence the optical and electronic properties of these antimony-corrole complexes. Nocera and co-workers first synthesized an oxo-bridged antimony(V) corrole dimer from an antimony(III) corrole upon reaction with the oxidizing agent iodosobenzene.[35] The resulting oxo-bridged antimony(V) corrole, (Cor)₂Sb₂^V-23a, was subsequently utilized as a photocatalyst for C–H activation. A detailed structural description of (Cor)₂Sb₂^V-23a and its role in C–H activation is provided below (vide infra). Following the procedure reported by Nocera et al. for the synthesis of oxo-bridged antimony(V) corrole dimers,[35] we have recently synthesized a related oxo dimer complex; 10-(4, 7-di-methoxynaphthalen-1-yl)-5, 15-bis(4-cyanophenyl)corrolato(oxo)antimony(V) dimer {(Cor)₂Sb₂^V-8a}.[36] The FB corroles 1,10-(pyrene-1-yl)-5,15-bis(4-cyanophenyl)corrole and 10-(4,7-di-methoxynaphthalen-1-yl)-5,15-bis(4- cyanophenyl)corrole, and their antimony(III) analogues; 10-(4,7-di-methoxynaphthalen-1-yl)-5,15-bis(4- cyanophe
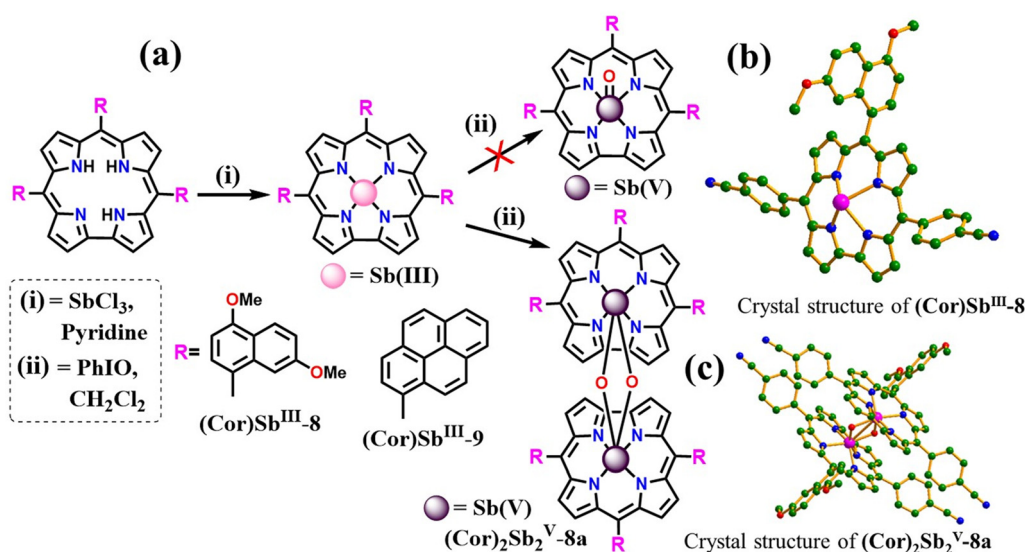

Fig. 3 (a) Molecular structure of different FB corroles, antimony(III)-corrole; {(Cor)Sb^III-8} and {(Cor)Sb^III-9}, and crystal structures of (b) (Cor)Sb^III-8 and (c) (Cor)₂Sb₂^V-8a. Adapted from ref. 36 with permission from John Wiley and Sons. © 2023 Wiley-VCH.

nyl)corrolato-antimony(III) {(Cor)Sb^{III}-8}, 1,10-(pyrene-1-yl)-5,15-bis(4-cyanophenyl)corrolatoantimony(III){(Cor)Sb^{III}-9} (Fig. 3) were synthesized following the procedure reported by Gross *et al.*[31]

All the synthesized antimony-corrole complexes (Fig. 3) were confirmed to be diamagnetic based on ^1H NMR spectroscopy, as evidenced by sharp peaks with normal chemical shifts. The crystal structures of (Cor)Sb^{III}-8 and (Cor)$_2$Sb$_2$^{V}-8a revealed a dome-shaped geometry (Fig. 3b and c), with all four Sb–N bond lengths closely matching previously reported similar complexes.[31,35] Interestingly, both antimony(III)-corrole complexes, (Cor)Sb^{III}-8 and (Cor)Sb^{III}-9, underwent oxidation to form dimeric oxo-antimony(v)-corrole complexes. However, a pure form was successfully obtained only for (Cor)$_2$Sb$_2$^{V}-8a. This observation highlights that substitutions at the *meso*-carbon in the corrole moiety significantly influence whether an oxo monomeric or dimeric complex is formed. As a key application, the singlet oxygen generation quantum yield of (Cor)$_2$Sb$_2$^{V}-8a was measured, yielding an impressive quantum efficiency of 69% upon light irradiation using 5,10,15,20-tetraphenyl-21H,23H-porphine as a reference.[36] This high quantum yield underscores the potential of these antimony-corrole complexes as efficient photosensitizers for applications such as photo-dynamic therapy (PDT) and photooxidation reactions.

Recently, Tschierlei *et al.* synthesized and characterized an A$_2$B-type corrole, {5,15-di(4-cyanophenyl)-10-(2,4,5-trimethoxyphenyl)corrole}, along with three different antimony(v)–corrole complexes featuring fluoro {(Cor)Sb^V-10}, chloro {(Cor)Sb^V-11}, and bromo {(Cor)Sb^V-12} substituents at the axial positions of the metal center (Fig. 4a).[37] All three complexes displayed intense Soret absorption bands between 418–428 nm, accompanied by weaker Q bands in the 608–623 nm region. Emission spectra in CH$_2$Cl$_2$ revealed fluorescence maxima at 624 nm for (Cor)Sb^V-10, 638 nm for (Cor)Sb^V-11, and 642 nm for (Cor)Sb^V-12, with corresponding emission quantum yields of 9.2%, 3.4%, and 2.0%, respectively. The emission quantum yields of (Cor)Sb^V-10, (Cor)Sb^V-11, and (Cor)Sb^V-12 were determined using [Ru(bpy)$_3$]Cl$_2$ in dichloromethane as a reference. These findings indicate that (Cor)Sb^V-10 exhibits the highest emissive efficiency, suggesting that fluoro substitution enhances both fluorescence quantum yield and photostability. Moreover, all three

complexes showed prolonged triplet excited-state lifetimes exceeding 20 μs, underscoring their efficiency in generating singlet oxygen. This property renders them highly suitable for catalytic photochemical applications. Among them, (Cor)Sb^V-10 demonstrated the highest singlet oxygen quantum yield (>95%), surpassing that of (Cor)Sb^V-11 (83%) and (Cor)Sb^V-12 (90%). The singlet oxygen quantum yields of (Cor)Sb^V-10, (Cor)Sb^V-11, and (Cor)Sb^V-12 were calculated using Perinaphtenone (assuming its singlet oxygen quantum yields = 1) as a reference.

The photochemical oxidation of 2,5-diphenylfuran to 1,2-dibenzoylethylene, mediated by singlet oxygen ($^1O_2$), was monitored using UV-vis spectroscopy during catalytic reactions employing (Cor)Sb^V-10. A gradual decrease in the absorption band at 328 nm, corresponding to the consumption of 2,5-diphenylfuran, was observed alongside the emergence of a new absorption peak at 255 nm, indicative of 1,2-dibenzoylethylene formation (Fig. 4b). Among the three antimony(v)–corrole complexes investigated, (Cor)Sb^V-10 displayed the highest catalytic efficiency, outperforming (Cor)Sb^V-11 and (Cor)Sb^V-12 in facilitating the photooxidation reaction.[37] This enhanced activity is attributed to its superior photophysical properties, particularly its elevated singlet oxygen quantum yield.

Nocera *et al.* synthesized an A$_2$B-type corrole, 10-(4-methoxycarbonylphenyl)-5,15-bis(pentafluorophenyl)corrole, and its corresponding antimony(III) complex, (Cor)Sb^{III}-13, following established synthetic protocols (Fig. 5a). The single-crystal X-ray structure of (Cor)Sb^{III}-13 revealed a pronounced dome-shaped conformation, with the Sb(III) center residing 0.974 Å above the mean corrole plane.[38] Subsequent oxidations of (Cor)Sb^{III}-13 with PhICl$_2$ yielded the dichloro antimony(v) complex (Cor)Sb^V-14, while treatment with Br$_2$ afforded the dibromo analog (Cor)Sb^V-15. The crystal structure of (Cor)Sb^V-14, obtained from CH$_2$Cl$_2$, confirmed a classical octahedral geometry in which two axial chloro ligands stabilize the Sb(v) center within the corrole framework.

The FB corrole, antimony(III)-corrole, and antimony(v)-corrole complexes were comprehensively characterized using a suite of spectroscopic techniques, including UV-vis and emission spectroscopy, which revealed no anomalous features under standard conditions. However, an unexpected
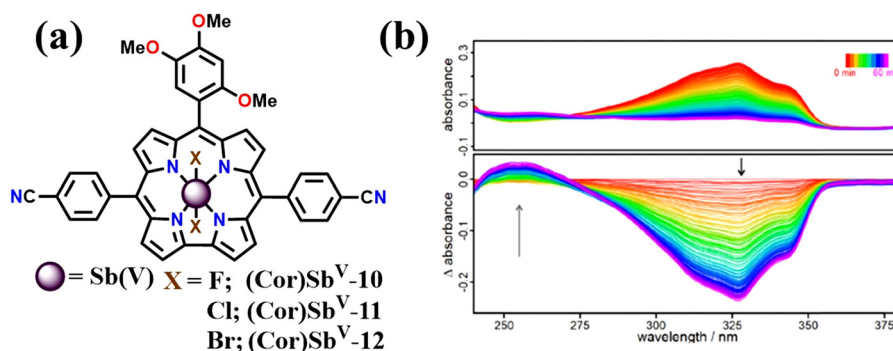
Fig. 4 (a) Structures of various halogen-substituted antimony(v) corroles; (b) *in situ* UV-vis spectra (top) and corresponding differential absorption spectra (bottom) showing the depletion of 2,5-diphenylfuran and formation of 1,2-dibenzoyl ethylene during the first hour of the photocatalytic oxidation reaction under irradiation with $\lambda > 400$ nm. Adapted from ref. 37 with permission from the Royal Society of Chemistry. © 2024 The Royal Society of Chemistry.
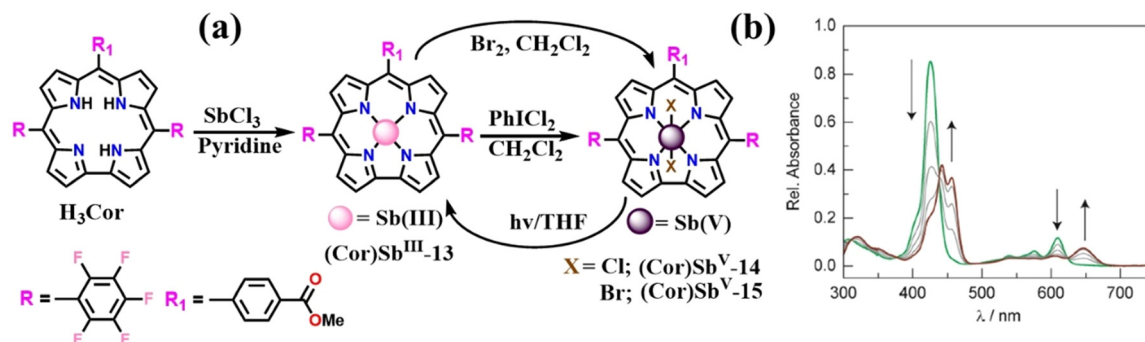
Fig. 5 (a) Molecular structure of FB corrole, antimony(III)-corrole; **(Cor)Sb^{III}-13**, antimony(v)-corroles; chloro substituted **(Cor)Sb^{V}-14** and bromo substituted **(Cor)Sb^{V}-15**, and (b) UV-vis spectra during the conversion of **(Cor)Sb^{V}-15** to **(Cor)Sb^{III}-13** in THF upon photo irradiation. Adapted from ref. 38 with permission from the American Chemical Society. © 2018 American Chemical Society.

photochemical transformation was observed for **(Cor)Sb^{V}-15** when exposed to light in tetrahydrofuran (THF). Upon irradiation at $\lambda > 305$ nm, **(Cor)Sb^{V}-15** underwent a photoreduction to yield **(Cor)Sb^{III}-13**. This transformation was tracked using UV-vis spectroscopy, wherein the characteristic green absorption spectrum of **(Cor)Sb^{V}-15** fully converted to the brown spectrum associated with **(Cor)Sb^{III}-13** (Fig. 5b). The observed Sb(v) → Sb(III) conversion is attributed to photoinduced elimination of the axial halide ligands.[38] Density Functional Theory (DFT) calculations performed on **(Cor)Sb^{V}-14** and **(Cor)Sb^{V}-15** indicated a substantial antibonding characteristic within the axial Sb–X bonds, rendering them relatively weak and photolabile, thus facilitating ligand dissociation under photonic excitation.

Corroles are known to form stable complexes with metal ions across a range of oxidation states, most commonly from +II to +V.[39–42] Recently, Bröring *et al.* synthesized two structurally distinct corroles: 5,15-dimesityl-10-(4-methoxyphenyl)corrole and 5,15-dimesityl-10-(2,4,6-trimethoxyphenyl)corrole.[43] The former contains a relatively less bulky aryl substituent, while the latter features a more sterically hindered methoxy-substituted aryl group. Both ligands were found to form stable antimony(III)-corrole complexes, **(Cor)Sb^{III}-16** and **(Cor)Sb^{III}-17**, respectively, upon reaction with SbCl$_3$ in pyridine (Fig. 6a).

The single-electron oxidation of antimony(III) corroles, **(Cor)Sb^{III}-16** and **(Cor)Sb^{III}-17**, with silver(I) perchlorate (AgClO$_4$) or silver triflate (AgOTf) in dry CH$_2$Cl$_2$ leads to the
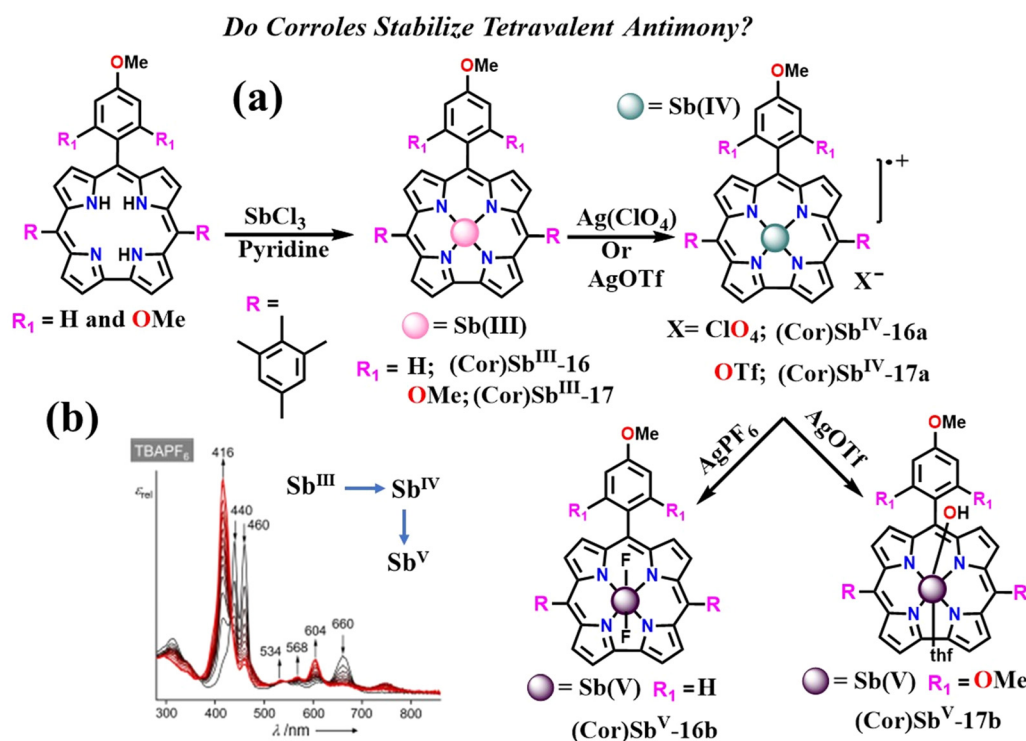

Fig. 6 (a) Metalo-corroles with +3, +4 and +5 oxidation states of antimony (Sb) metal ion, and (b) UV-vis spectroscopic investigations during the conversion of Sb^{III} to Sb^{IV} to Sb^{V}. Adapted from ref. 43 with permission from John Wiley and Sons. © 2023 Wiley-VCH.

formation of antimony(IV) corroles, **(Cor)Sb^{IV}-16a** and **(Cor)Sb^{IV}-17a**. Crystallographic analysis of **(Cor)Sb^{III}-16** and **(Cor)Sb^{IV}-16a** reveals largely similar structural parameters, with the principal difference being the presence of a perchlorate anion in **(Cor)Sb^{IV}-16a** and a disordered solvent molecule in **(Cor)Sb^{III}-16**. Both complexes adopt dome-shaped geometries, with the Sb center displaced by 0.971 Å in **(Cor)Sb^{III}-16** and 1.017 Å in **(Cor)Sb^{IV}-16a** above the corrole plane. Further oxidation of **(Cor)Sb^{IV}-16a** and **(Cor)Sb^{IV}-17a** using excess AgPF$_6$ in CH$_2$Cl$_2$ or AgOTf in THF containing trace water afforded the most stable antimony(V) corrole complexes, **(Cor)Sb^{V}-16b** and **(Cor)Sb^{V}-17b**.[43] The redox progression from Sb(III) to Sb(IV) and subsequently Sb(V) in these corrole complexes was systematically monitored by UV-vis spectroscopy (Fig. 6b). These findings illustrate that corrole ligands effectively stabilize antimony across multiple oxidation states (+3, +4, and +5), underscoring their versatility in modulating metal oxidation states. The general introduction outlines the molecular properties of antimony(III/V) corrole complexes, while their reactivity and diverse applications are discussed in detail in the subsequent sections.

2. Reactivities of antimony(III/V)-corrole complexes

Most macrocyclic ligands are inherently redox-active, enabling them to participate in a wide range of chemical transformations.[44–46] Upon coordination with metal centers, the redox properties of these ligands are often amplified due to synergistic interactions between the metal and the macrocycle, enhancing the overall reactivity of the resulting complexes. Among such ligands, corroles have garnered considerable interest due to their remarkable ability to stabilize high-valent metal centers.[47–50] This capability renders corrole complexes particularly valuable, as high oxidation state metal ions are frequently employed as oxidants in diverse redox processes. Gross and co-workers reported the synthesis of a pentafluorophenyl-substituted corrole, 5,10,15-tris(pentafluo-

rophenyl)corrole, along with its antimony(III) complex prepared *via* the reaction of SbCl$_3$ in pyridine.[31] The resulting antimony(III) corrole complex was further oxidized to afford the corresponding antimony(V) species, **(Cor)Sb^{V}-3**. Initially, **(Cor)Sb^{V}-3** was evaluated as a photocatalyst for the oxidative transformation of bromide to bromine under illumination with a "sunlight" lamp (250 W, Osram). The catalytic turnover frequency (TOF) for bromine generation was measured to be 35 h^{-1}.[51] Subsequently, replacing the sunlight source with a blue light-emitting diode (LED; λ_{em} = 450 nm, power = 150 mW cm^{-2}) resulted in a significant enhancement in catalytic performance, achieving a TOF of 72 h^{-1} using **(Cor)Sb^{V}-3** as the photocatalyst. The TOF of a catalyst refers to its catalytic activity, specifically indicating the number of reactions completed per unit time by a single active site of the catalyst.

Modifying the corrole periphery by introducing bromine atoms at the β-positions yields **H$_3$CorBr$_8$** (Fig. 7a), which was further complexed with antimony(V) to form **(Cor)Sb^{V}-18**. Bromination at the β-positions significantly influences the electronic properties, redox potentials, and overall stability of the resulting corrole complexes.[51] Brominated corrole derivatives have also been shown to form robust complexes with Al(III), Ga(III), and P(V) ions, leading to the synthesis of **(CorBr$_8$)Al^{III}**, **(CorBr$_8$)Ga^{III}**, and **(CorBr$_8$)P^{V}** *via* established synthetic protocols. These metallocorroles were evaluated as photocatalysts for the bromide-to-bromine transformation and exhibited substantial TOF: 290 h^{-1} for **(CorBr$_8$)Al^{III}**, 341 h^{-1} for **(CorBr$_8$)Ga^{III}**, and 93 h^{-1} for **(CorBr$_8$)P^{V}**. The efficiency of this photo-catalyzed reaction is attributed to the generation of singlet oxygen (^{1}O$_2$) upon photoexcitation (Fig. 7b). Notably, the incorporation of bromine enhances spin–orbit coupling, thereby promoting intersystem crossing (ISC) and facilitating efficient ^{1}O$_2$ generation. Kar *et al.* recently synthesized two antimony(III) corroles based on previously reported FB corroles-5,10,15-triphenylcorrole and 5,10,15-tris(4-methoxyphenyl)corrole-by following established procedures.[52] The FB corroles and their antimony(III)-corroles; **(Cor)Sb^{III}-19** and **(Cor)Sb^{III}-20** were characterised by ^{1}H NMR, ESI-MS, IR, UV-Vis and emission spectroscopies. Interestingly, both the
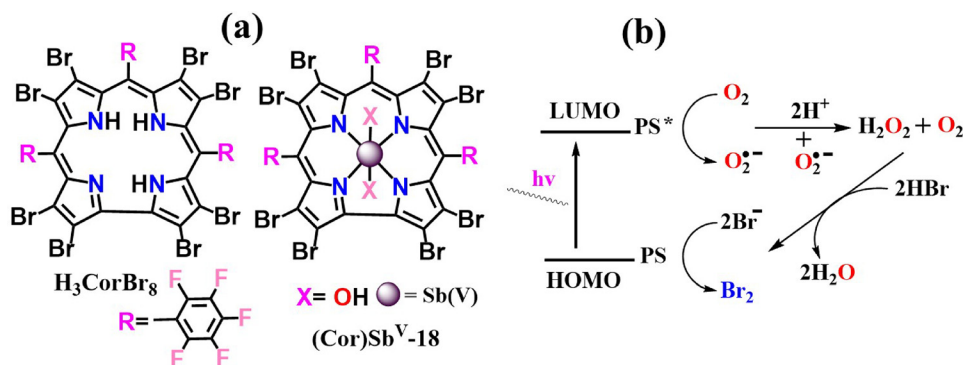

Fig. 7 (a) Molecular structure of bromo substituted corrole (**H$_3$CorBr$_8$**) and its antimony(V)-corrole {**(Cor)Sb^{V}-18**}, and (b) proposed mechanism for the photocatalytic oxidation of bromide to bromine during photo-excitation of metallocorroles. Adapted from ref. 51 with permission from John Wiley and Sons. © 2015 Wiley-VCH.

antimony(III)-corroles; **(Cor)Sb**^{III}**-19** and **(Cor)Sb**^{III}**-20** were reactive with nitrosonium tetrafluoroborate ($NOBF_4$) in the presence of air, leading to the formation of *trans*-difluoroantimony(v) 3,17-dinitro-corrole complexes; **(Cor)Sb**^{III}**-19a** and **(Cor)Sb**^{III}**-20a** (Fig. 8a).

Similarly, treating with NO gas in a CH_2Cl_2–CH_3CN solvent mixture in the presence of air, the antimony(III)-corrole **(Cor)Sb**^{III}**-19** formed (oxo)antimony(v)-corrole complex **(Cor)Sb**^{III}**-19b**. However, no successful reaction was observed when **(Cor)Sb**^{III}**-19** is treated with $NOClO_4$ in a CH_2Cl_2–CH_3CN solvent mixture in the presence of air. Both the *trans*-difluoroantimony(v) 3,17-dinitro-corrole complexes; **(Cor)Sb**^{III}**-19a** and **(Cor)Sb**^{III}**-20a** showed similar absorption and emission peaks, a Soret band was observed in the range of 423–454 nm and three Q-bands were observed in the range of 543–665 nm (Fig. 8b). The transformation of antimony(III)-corroles, **(Cor)Sb**^{III}**-19** and **(Cor)Sb**^{III}**-20**, to their trans-difluoroantimony(v) 3,17-dinitro-corrole complexes, **(Cor)Sb**^{III}**-19a** and **(Cor)Sb**^{III}**-20a**, by $NOBF_4$ went through several intermediate steps, and all the intermediate products were completely characterised by various spectroscopic techniques. In addition, the complexes **(Cor)Sb**^{III}**-19a** and **(Cor)Sb**^{III}**-20a** were employed as photocatalysts for oxygenation reactions of aromatic compounds in air by *in situ* formation of singlet oxygen.[52] Given that corroles and their metal analogues are redox-active compounds, structural modifications, such as the introduction of functionalized anchoring groups, may enhance their photocatalytic performance and support the development of more efficient materials for future applications.

Antimony(III/v)-corrole complexes in biomedical applications

As previously discussed in the general section, the corrole macrocycle is structurally analogous to porphyrins and corrins.[53–55] Both porphyrins and corrins, along with their metal derivatives, are extensively employed in numerous biological systems.[56] Accordingly, it is unsurprising that corroles and metallo-corroles have emerged as bioactive compounds, particularly as potent photosensitizers in photodynamic therapy (PDT) for cancer treatment.[57–60] For instance, Gross and co-workers have recently developed gallium(III)-corrole-based nanoparticles for the treatment of castration-resistant prostate cancer.[61] These nanoparticles also exhibited potential as sonodynamic therapeutic agents for pancreatic cancer. Beyond Ga(III)-corroles, various other metallo-corroles have similarly demonstrated promising anticancer properties.[62] In medicinal chemistry, metal ion incorporation or ligand coordination is a widely adopted strategy to design pharmacologically active compounds. While certain organic scaffolds may exhibit limited bioactivity, these limitations can often be overcome by metal complexation. Notably, the FB corrole ligand itself is redox-active and capable of generating singlet oxygen, a key attribute in PDT-based cancer therapies.[63]

This further underscores the therapeutic versatility of corrole-based architectures in biomedical applications. The following section focuses on the biological utility of antimony(III/v)-corrole complexes. Annegret Preuß and co-workers designed and synthesized both positively and negatively charged antimony(v)- and phosphorus(v)-corroles for the photodynamic inactivation of mold fungi (Fig. 9a).[64] Mold fungi pose significant health risks, including respiratory tract diseases that may lead to malignant cell development. The synthesized antimony(v)-corroles exhibited excellent water solubility, photostability, and exceptionally high singlet oxygen quantum yields upon light irradiation. These properties rendered them effective for targeted photodynamic inactivation of mold fungi,
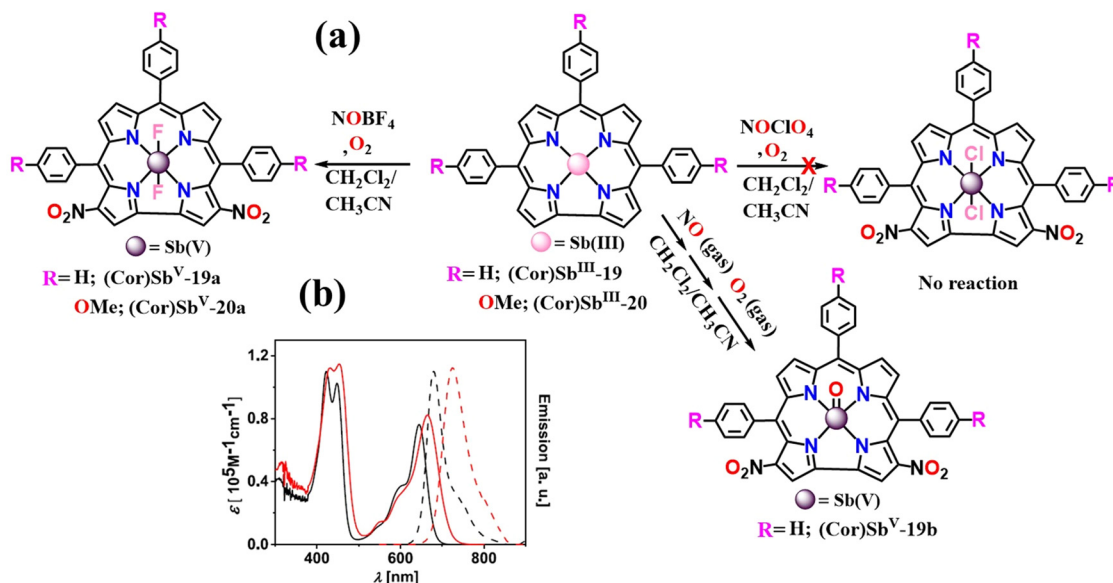
Fig. 8 (a) Molecular structure of antimony(III)-corroles; **(Cor)Sb**^{III}**-18** and **(Cor)Sb**^{III}**-19**, and their reactivity with different reagents, and (b) absorption (solid lines) and emission (dashed lines) spectra of **(Cor)Sb**^{III}**-18** (black line) and **(Cor)Sb**^{III}**-19** (red line) in aerated dichloromethane. Adapted from ref. 52 with permission from John Wiley and Sons. © 2023 Wiley-VCH.
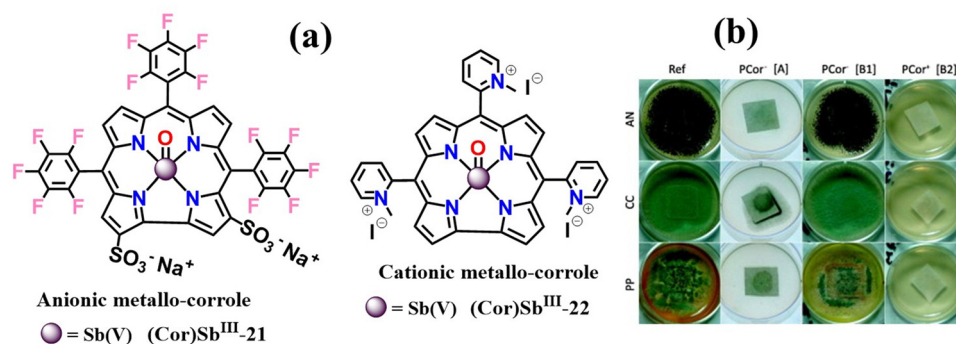
Fig. 9 (a) Molecular structure of cationic and anionic antimony(v)-corroles; **(Cor)Sb^V-21** and **(Cor)Sb^V-22**, and (b) their phototoxicity against *Aspergillus niger* (top line), *Cladosporium cladosporoides* (middle line), ore *Penicillium purpurgenum* (bottom line). Adapted from ref. 64 with permission from Elsevier. © 2014 Elsevier.

including *Aspergillus niger* (AN), *Cladosporium cladosporoides* (CC), and *Penicillium purpurgenum* (PP) (Fig. 9b). In Fig. 9b, the "Ref" column represents the growth of AN, CC, and PP fungi after three days of incubation under illumination in the absence of phosphorus(v)-corroles. Column 'A' shows the characteristic growth inhibition of AN, CC, and PP when incubated with the anionic phosphorus(v)-corroles. In contrast, column 'B1' illustrates the recovery of these fungi following an additional incubation period in darkness. The column 'B2' presents the photodynamic effect of phosphorus(v)-corroles on the fungi.[64] No visible growth of the mold fungi was observed after 3 days of illumination and the subsequent incubation period in darkness. Similar kinds of inhibition of growth of mold fungi were observed upon photoactivation of antimony(v)-corroles induced lethal damage to fungal conidia (spores), which are the primary vectors for mold propagation. Importantly, none of the complexes exhibited toxicity under dark conditions, confirming the light-dependent nature of the antifungal activity. Among the derivatives, the cationic antimony(v)-corroles demonstrated superior photosensitizing efficacy, achieving complete inactivation of fungal conidia under irradiation.[64] The PDT antitumor activity of corroles and metallo-corroles is commonly evaluated using the MTT (methylthiazolyldiphenyl-tetrazolium bromide) assay, which assesses cell viability by measuring the reduction of MTT by succinate dehydrogenase in metabolically active (living) cells.[65] It is well established that corroles act as effective photosensitizers in photodynamic therapy (PDT); therefore, their main group element–corrole complexes are also expected to serve as promising photosensitizers. However, the photodynamic antitumor activity exhibited by various metallo-corroles has been shown to depend strongly on the molecular structure of the corrole, the nature of the central metal ion, and the specific cell lines used in evaluation.[66] For instance, corroles bearing pyridyl substituents have demonstrated notable PDT activity against different tumor cells, but also exhibited dark cytotoxicity with IC$_{50}$ values ranging from 4.68 to 0.59 μmol L^{-1} in HeLa cells.[67] The raised dark cytotoxicity of pyridyl-corroles is attributed to their high cellular uptake in buffer solution. In contrast, hydroxyl-corrole and its gallium(iii) complex showed low dark cytotoxicity but

high photocytotoxicity toward A549, BEL-7402, and SiHa cell lines.[68] Similarly, a phosphorus(iii)-corrole bearing a methyl benzoate functional group exhibited low dark toxicity toward H460 and A549 cell lines (IC$_{50}$ > 80 μmol L^{-1}). However, upon exposure to a moderate light doses it exhibited high photocytotoxicity with IC$_{50}$ values of 1.2 μmol L^{-1} and 1.7 μmol L^{-1} for H460 and A549 cells, respectively.[69] Additionally, a tin(iv) complex of a tri-benzoate methyl ester-functionalized corrole exhibited moderate photocytotoxicity (approximately 40 μmol L^{-1}) against A549 cells.[70]

Therefore, to achieve efficient PDT activity with low dark cytotoxicity, high cellular selectivity, and improved aqueous solubility researchers should focus on modifying the corrole moiety or incorporating suitable metal ions into the corrole framework. As Sb(iii)/Sb(v) corrole complexes[36] have already been established as efficient generators of singlet oxygen—a key reactive species in PDT—this opens new avenues for developing biocompatible effective photosensitizers by structurally modifying the Sb(iii)/Sb(v) corrole framework. The above comparative study between antimony–corrole and other main group–corrole complexes highlights their differences and limitations. This analysis may serve as a valuable guide for future researchers in designing more efficient and biocompatible photosensitizers based on main group corrole complexes for photodynamic therapy (PDT).

3. Antimony(iii/v)-corrole complexes in C−H activation reactions

The synthesis of chemical compounds has long driven advancements across diverse scientific disciplines, from materials science to medicine, profoundly impacting and simplifying modern life.[71] Over the years, chemists have developed numerous synthetic strategies – including cross-coupling, rearrangement, substitution, and elimination reactions. Among these, C–H activation has gained considerable traction due to its efficiency and versatility.[72] Facilitated by metal ion catalysts, C–H activation enables the formation of target molecules with high yields and fewer synthetic steps.[73] Beyond individual

metal ions, metal complexes have emerged as powerful catalysts in C–H functionalization reactions.[74] These complexes offer improved control over metal reactivity and enable selective transformations, including stereoselective and regioselective product formation.[75] More recently, macrocyclic ligands such as porphyrins, corroles, and corins – and their corresponding metal complexes – have garnered attention for their unique roles in C–H activation, organic transformations, and small molecule activation.[76–81] In line with this, the current review focuses on the C–H activation potential of antimony(III/V) corrole complexes. For instance, an antimony(III)-corrole complex, **(Cor)Sb^{III}-23**, was synthesized by the Nocera group *via* complexation of a FB corrole with SbCl$_3$ in the presence of pyridine.[35] The complex was fully characterized using a suite of spectroscopic techniques, including single-crystal X-ray diffraction. The weakly emissive **(Cor)Sb^{III}-23** displayed an emission maximum at 669 nm and a shoulder at 730 nm in toluene. Its UV-vis spectrum featured a Soret band near 460 nm and Q-bands in the 570–700 nm range. Notably, upon treatment with various oxidants – such as H$_2$O$_2$–urea (74% yield), PhI(OAc)$_2$/O$_2$ (56% yield), or PhIO (71% yield) – **(Cor)Sb^{III}-23** was transformed into an oxo-bridged antimony(V) dimer, **(Cor)$_2$Sb$_2^V$-23a**, in varying yields (Fig. 10a). X-ray crystallographic analysis of **(Cor)$_2$Sb$_2^V$-23a** confirmed the absence of direct Sb–Sb and O–O bonds, with Sb···Sb and O···O separations of ∼3.0 Å and ∼2.5 Å, respectively, well beyond typical bonding distances. Upon dimer formation, the photophysical properties of the complex changed significantly: the weak emission of **(Cor)Sb^{III}-23** was enhanced in **(Cor)$_2$Sb$_2^V$-23a**, with an emission peak at 610 nm and a quantum yield increase from 0.013% to 0.13%. The relative quantum yields of **(Cor)Sb^{III}-23** and **(Cor)$_2$Sb$_2^V$-23a** were calculated using Nile blue as a reference (emission quantum yields = 0.27). This dramatic enhancement highlights the impact of oxidation state and molecular architecture on the optical properties of antimony corrole systems.

Beyond their photophysical properties, the dimeric complex **(Cor)$_2$Sb$_2^V$-23a** was evaluated as a photocatalyst for the selective oxidation of toluene to benzaldehyde under UV-Vis light irradiation ($\lambda_{exc} > 305$ nm).[35] The C–H activation reactions were performed under both aerobic and anaerobic conditions. In aerobic conditions, the oxidation of toluene proceeded in the presence of **(Cor)$_2$Sb$_2^V$-23a**; however, spectroscopic evidence for the reduction of the catalyst back to the antimony(III) complex; **(Cor)Sb^{III}-23** was inconclusive. In contrast, under anaerobic conditions, the catalytic conversion of toluene to benzaldehyde was accompanied by the clear transformation of **(Cor)$_2$Sb$_2^V$-23a** to **(Cor)Sb^{III}-23**, as monitored by UV-Vis spectroscopy in benzene (Fig. 10b). Interestingly, **(Cor)$_2$Sb$_2^V$-23a** selectively activated the benzylic C–H bond of toluene (bond dissociation energy ≈ 88.5 kcal mol^{-1}), but failed to oxidize substrates with either lower or higher bond dissociation energies, such as 1,3-cyclohexadiene (74.3 kcal mol^{-1}) and benzene (112.9 kcal mol^{-1}). This indicates that **(Cor)$_2$Sb$_2^V$-23a** exhibits high substrate selectivity toward toluene over other competitive hydrocarbons under identical reaction conditions. Recently, we have synthesized a new series of antimony(III) corroles: **(Cor)Sb^{III}-24**, **(Cor)Sb^{III}-25**, and **(Cor)Sb^{III}-26** based on a common tetrakis(thiocyano)corrole scaffold featuring four SCN groups at the β-positions of the macrocycle.[82] All three complexes were fully characterized using FT-IR, ESI-MS, ^{1}H NMR, UV-vis, and emission spectroscopy. Additionally, the molecular structure of **(Cor)Sb^{III}-25** was determined by single-crystal X-ray diffraction and further optimized by DFT calculations (Fig. 11). The incorporation of thiocyano groups at the β-positions resulted in pronounced red shifts (≈ 30–40 nm) in both absorption and emission spectra compared to the unsubstituted β-free corrolatoantimony(III) derivatives. Moreover, the Q-band intensities in these complexes were significantly enhanced, reaching approximately 70% of the Soret band intensities.

The β-substitution effectively extended the π-conjugation, enabling strong absorption in the far-red region (700–720 nm), which may enhance their applicability in light-driven applications. Furthermore, these antimony(III)-corrole complexes were employed as catalysts for the electrochemical oxidation of
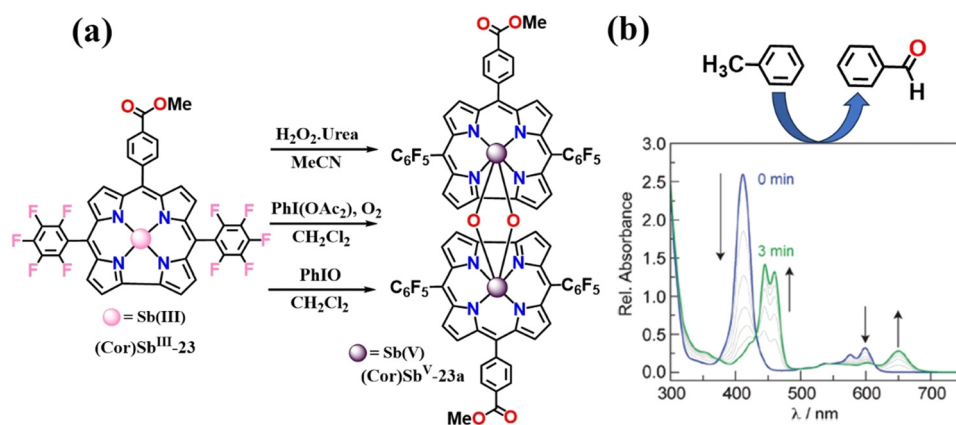

Fig. 10 (a) Molecular structure of antimony(III) and antimony(V)-corroles, and (b) how antimony(V)-corrole converts to antimony(III)-corrole during the catalytic transformation of toluene to benzaldehyde. Adapted from ref. 35 with permission from the Royal Society of Chemistry. © 2020 The Royal Society of Chemistry.
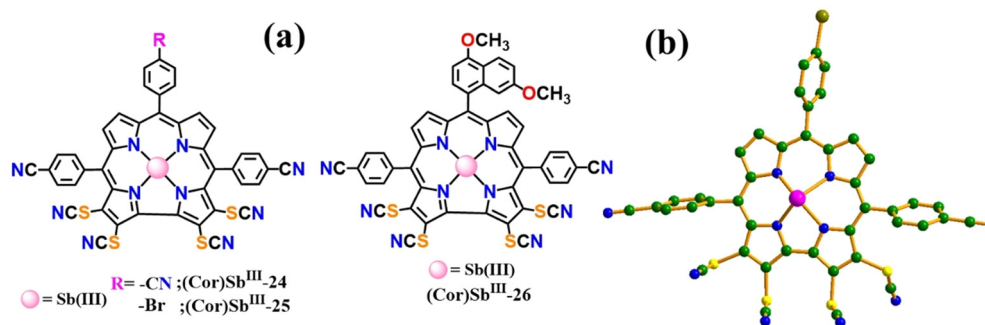
Fig. 11 (a) Molecular structure of β substituted antimony(III)-corroles, and (b) crystal structure of **(Cor)Sb^{III}-25**. Adapted from ref. 82 with permission from the American Chemical Society. © 2023 American Chemical Society.

benzyl alcohol to benzoic acid. In particular, **(Cor)Sb^{III}-26** was immobilized on nickel foam (NF) to prepare the electrocatalytic composite **(Cor)Sb^{III}-26@NF**. The electrochemical performance of this system was evaluated using cyclic voltammetry (CV) and linear sweep voltammetry (LSV) in aqueous KOH solution. The LSV results revealed that **(Cor)Sb^{III}-26@NF** exhibits excellent catalytic activity toward both the oxygen evolution reaction (OER) and the electrooxidation of benzyl alcohol. These findings highlight the potential of β-substituted antimony(III)-corroles as multifunctional electrocatalysts for oxidative transformations under mild conditions.

The **(Cor)Sb^{III}-26@NF** catalyst required an overpotential of 360 mV to achieve a catalytic current density of 50 mA cm^{-2}, which is significantly lower than that of bare nickel foam (NF), as shown in Fig. 12a.[82] The term 'overpotential' refers to the excess potential, beyond the thermodynamic equilibrium value, required to drive an electrochemical reaction at an observable rate.

The electrocatalytic oxidation of benzyl alcohol using **(Cor)Sb^{III}-26@NF** proved to be highly efficient compared to conventional oxidation methods for converting benzyl alcohol to benzoic acid. During the catalytic process, the antimony(III)-corrole complex **(Cor)Sb^{III}-26** undergoes electrochemical oxidation to form a high-valent Sb^V = O corrole species. This *in situ* generated oxo-antimony(v) complex is believed to facilitate both

the oxygen evolution reaction (OER) and the selective activation of the benzylic C–H bond, ultimately yielding benzoic acid (Fig. 12b). Currently, our research is directed toward the development of a new class of antimony(III/v)-corrole complexes through structural modifications of the corrole macrocycle and incorporation of auxiliary functional groups. These efforts aim to further enhance their catalytic performance in OER, C–H activation, and small molecule activation processes.

4. Antimony(III/v)-corrole complexes in the H$_2$ evolution reaction

The rising global population and the progressive depletion of fossil fuel reserves have intensified the pursuit of alternative, sustainable energy sources. Among these, hydrogen (H$_2$) has emerged as a particularly promising candidate due to its high gravimetric energy density (142 MJ kg^{-1}) and carbon-neutral combustion profile, rendering it an attractive energy vector for a sustainable future.[83] The hydrogen evolution reaction (HER), a key step in hydrogen production, is typically facilitated by metal-ion-based organic catalysts whose catalytic efficiencies can be fine-tuned through rational ligand design and structural modifications.[84,85] Currently, noble metal-based catalysts dominate the field due to their exceptional activity; however, their
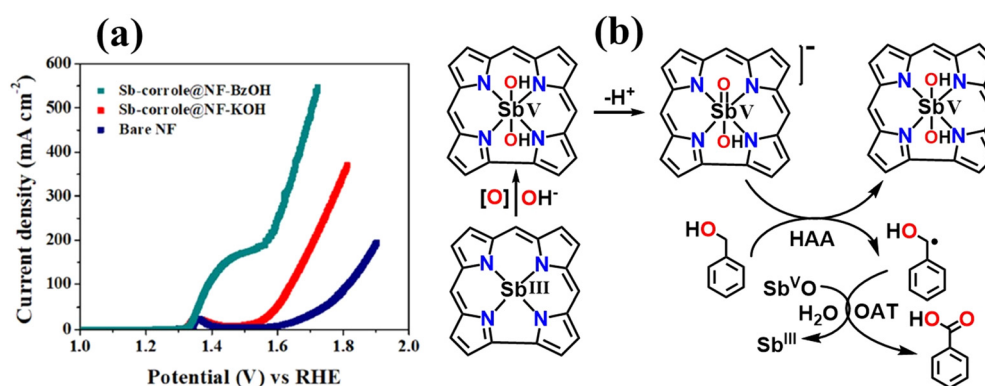

Fig. 12 (a) Linear-sweep voltammetry (LSV) of **(Cor)Sb^{III}-26@NF** in KOH and benzyl alcohol (BzOH) solutions and (b) mechanism for the catalytic transformation of benzyl alcohol to benzoic acid. Adapted from ref. 82 with permission from the American Chemical Society. © 2023 American Chemical Society.

high cost, scarcity, and issues with long-term operational stability pose critical limitations.[86] In response to these challenges, considerable research has focused on first-row transition metal complexes bearing redox-active ligands, which offer promising HER activity coupled with enhanced affordability and durability.[87] Recent developments have also highlighted the potential of main-group elements coordinated with redox-active ligands as effective HER catalysts.[88] In a notable study, Jiang *et al.* investigated porphyrin–Sb^V(OH)$_2$ complexes as electrocatalysts for the HER under acidic conditions, underscoring the viability of antimony-based systems in this context.[89] Porphyrins, recognized for their inherent redox versatility and strong coordination capabilities, have been extensively explored for HER catalysis. Metallo-porphyrins[90] and their corrole analogues[91] are increasingly being recognized as potent catalytic systems for both HER and water oxidation. These advancements collectively contribute to the development of cost-effective, robust, and earth-abundant catalytic platforms for sustainable hydrogen production, providing viable alternatives to noble metal-based technologies.

Recently, three distinct antimony(III)-corrole complexes, each incorporating a nitro group at the *ortho-*, *meta-*, or *para*-position of the 10-phenyl substituent on the corrole scaffold, **(Cor)Sb^{III}-27**, **(Cor)Sb^{III}-28**, and **(Cor)Sb^{III}-29** (Fig. 13a), were synthesized and comprehensively characterized through various spectroscopic and single-crystal X-ray diffraction techniques.[92] Crystallographic analysis of **(Cor)Sb^{III}-27** and **(Cor)Sb^{III}-28** (Fig. 13b and c) revealed that the Sb–N bond lengths fall within the range of 2.113–2.142 Å for **(Cor)Sb^{III}-27** and 2.119–2.132 Å for **(Cor)Sb^{III}-28**, indicating subtle structural variations influenced by the electronic and steric effects of the nitro group positioning on the phenyl ring.

The displacement of the Sb(III) center from the corrole macrocycle plane was determined to be 0.9797 Å for **(Cor)Sb^{III}-27** and 0.9799 Å for **(Cor)Sb^{III}-28**. The oxidation state of antimony was confirmed *via* UV-vis spectroscopy, which exhibited a characteristic Soret band at 425 nm and three Q-bands spanning with the range 530–650 nm, consistent with reported spectral features of antimony(III)-corroles.[35] The three antimony(III)-corrole complexes, **(Cor)Sb^{III}-27**, **(Cor)Sb^{III}-28**, and **(Cor)Sb^{III}-29**, were evaluated as electrocatalysts for the hydrogen evolution reaction (HER) in both acetonitrile and neutral aqueous buffer systems, using acetic acid

(AcOH), trifluoroacetic acid (TFA), and *p*-toluenesulfonic acid (TsOH) as proton sources. All three complexes displayed notable electrocatalytic activity, with the catalytic performance following the trend: **(Cor)Sb^{III}-27** > **(Cor)Sb^{III}-28** > **(Cor)Sb^{III}-29**. In particular, **(Cor)Sb^{III}-27** demonstrated an impressive TOF of 17.65 s^{-1} in acetonitrile using TFA as the proton source at an overpotential of 642 mV.

Electrolyte solution resistance (R_s) for all three complexes was measured using Nyquist plots under conditions of 38 equivalents of trifluoroacetic acid (TFA) at −1.9 V and 38 equivalents of *p*-toluenesulfonic acid (TsOH) at −1.6 V. The Nyquist plots (Fig. 14a) revealed consistent electrolyte resistance values of approximately 10 Ω under both acidic conditions, indicating minimal variation in ion transport resistance across the systems. Based on various electrochemical and spectroscopic observations, it was concluded that protonation, followed by the reduction of the [Sb^{III}-corrole] complex to [Sb^{III}-corrole]$^-$, constitutes the key mechanistic step in the hydrogen evolution reaction (HER) pathway (Fig. 14b).[92] The electron transfer kinetics of the catalyst were investigated using electrochemical impedance spectroscopy (EIS). Among the tested complexes **(Cor)Sb^{III}-27**, **(Cor)Sb^{III}-28**, and **(Cor)Sb^{III}-29**, complex **(Cor)Sb^{III}-27** exhibited the lowest charge transfer resistance (R_{ct}), measuring 324 Ω in TFA and 310 Ω in TsOH, indicating superior electron-transfer kinetics and enhanced interfacial conductivity. This improved conductivity correlates with the highest catalytic current and TOF observed for complex **(Cor)Sb^{III}-27**.[92] The diffusion-controlled nature of the redox event, confirmed by the linear Randles–Sevcik relationship between peak current (i_p) and the square root of scan rate ($v^{1/2}$), suggests that electron transfer precedes protonation in a kinetically competent manner. Moreover, the shifts in reduction potentials and catalytic currents upon acid addition further implicate electron transfer at the [Sb(III)-corrole]/[Sb(III)-corrole]$^-$ redox couple is a kinetically significant step that likely influences the overall catalytic efficiency.[92]

Gross *et al.* synthesized three structurally distinct antimony(III) corroles, **(Cor)Sb^{III}-30**, **(Cor)Sb^{III}-31**, and **(Cor)Sb^{III}-32**, each bearing different *meso*-carbon substituents on the corrole macrocycle (Fig. 15a).[93] Specifically, **(Cor)Sb^{III}-30** features the smallest and most electron-withdrawing CF$_3$ groups, **(Cor)Sb^{III}-31** incorporates the commonly studied –C$_6$F$_5$ substituents, and **(Cor)Sb^{III}-32** carries
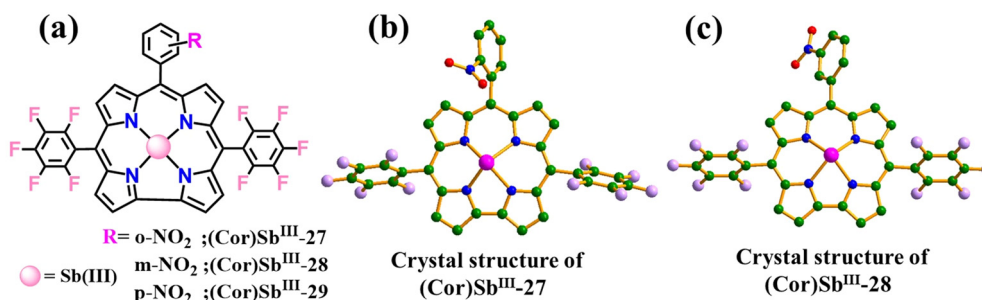

Fig. 13 (a) Molecular structure of antimony(III)-corroles, and crystal structure of (b) **(Cor)Sb^{III}-27** and (c) **(Cor)Sb^{III}-28**. Adapted from ref. 92 with permission from the Royal Society of Chemistry. © 2024 The Royal Society of Chemistry.
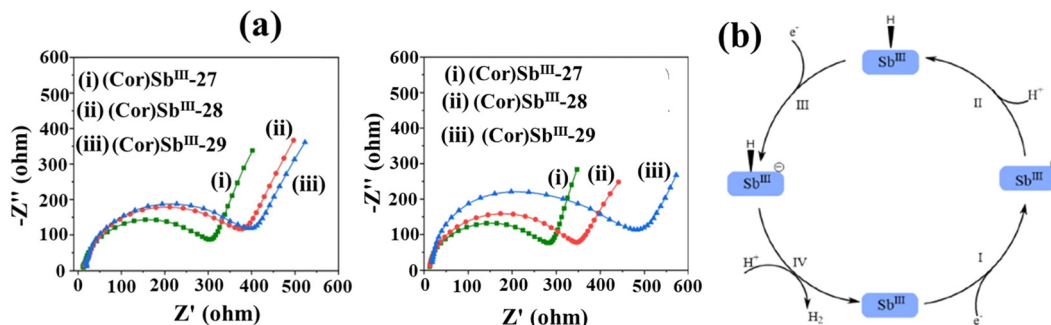
Fig. 14 (a) Nyquist plots of 0.2 mM antimony (III)-corroles with 38 eq. TFA (i) and 38 eq. TsOH (ii) in CH$_3$CN and (b) the proposed mechanism for electrocatalytic HER with antimony (III)-corroles. Adapted from ref. 92 with permission from the Royal Society of Chemistry. © 2024 The Royal Society of Chemistry.

the large, electron-donating 2,6-dimethoxyphenyl groups. All three complexes, along with their corresponding FB corroles, were thoroughly characterized using high-resolution mass spectrometry, UV-Vis spectroscopy, ^{1}H NMR, and elemental analysis. Furthermore, the crystal structure of **(Cor)Sb^{III}-32**, obtained from a 1:1 (v/v) CH$_2$Cl$_2$/n-heptane solvent mixture, revealed four Sb–N bond lengths of 2.112, 2.108, 2.120, and 2.119 Å. The structure confirmed a dome-shaped macrocycle with the antimony(III) center positioned 0.951 Å above the mean plane defined by the coordinating nitrogen atoms.

Substitution at the *meso*-carbon positions of the corrole macrocycle significantly influences the reduction half-wave potentials ($E_{1/2}$) of the corresponding antimony(III) corroles. The reduction potentials were determined to be −1.73 V for **(Cor)Sb^{III}-32**, −1.59 V for **(Cor)Sb^{III}-31**, and −1.31 V for **(Cor)Sb^{III}-30** *versus* ferrocene, reflecting the increasing electron-withdrawing nature of the *meso*-substituents in the order 2,6-dimethoxyphenyl < C$_6$F$_5$ < CF$_3$.[93] These antimony(III) corrole complexes were evaluated as electrocatalysts for the hydrogen evolution reaction (HER) in acetonitrile using trifluoroacetic acid (TFA) as the proton source. Their catalytic

activity was benchmarked against that of the less reactive boron subphthalocyanine analogues, and the key intermediates were geometrically optimized *via* density functional theory (DFT) calculations. Comparative experimental and computational studies led to several important mechanistic insights: (i) proton-to-hydrogen conversion occurs at potentials lower than those required for the one-electron reduction of the complexes in the absence of acid; (ii) a second proton reacts with the one-electron-reduced antimony(III) complex (Fig. 15b); (iii) the antimony center does not participate in proton binding; and (iv) the preferred protonation sites are the *meso*-carbon and peripheral nitrogen atoms of both corrole and subphthalocyanine macrocycles.[93] In a related study, Kar *et al.* designed a FB corrole incorporating hydrogen-bonding functionalities to enhance interactions with water molecules, thereby facilitating the hydrogen evolution reaction (HER) upon coordination to metal centers. The corresponding antimony(III) corrole complex was synthesized *via* complexation with SbCl$_3$ in the presence of pyridine. Oxidation of this complex using iodobenzene diacetate (PhIO) yielded an oxo-bridged antimony(V) corrole dimer,
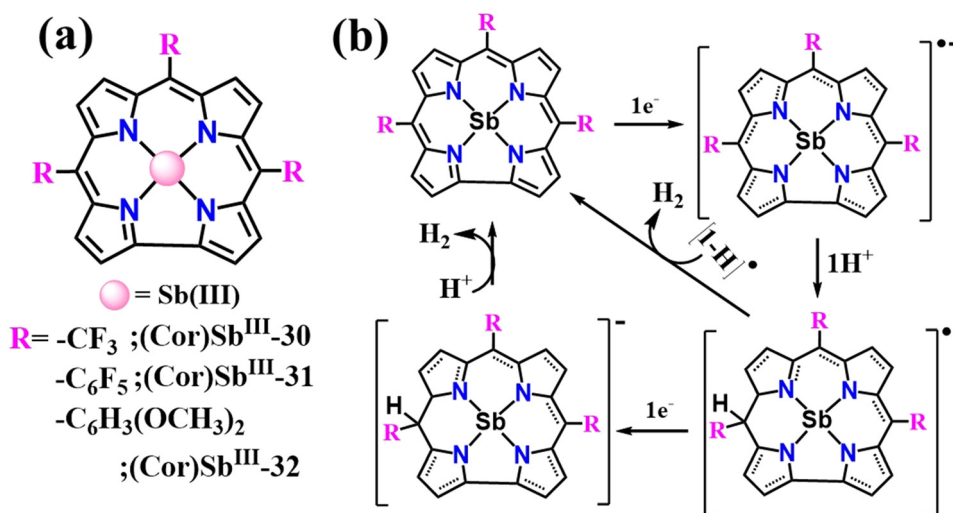

Fig. 15 (a) Molecular structure of antimony(III)-corroles with different *meso*-C substituents, and (b) proposed mechanism for hydrogen evolution by these antimony(III)-corroles. Adapted from ref. 93 with permission from John Wiley and Sons. © 2024 Wiley-VCH.

(Cor)$_2$Sb$_2$^{V}-33.[94] Single-crystal X-ray diffraction analysis of **(Cor)$_2$Sb$_2$^{V}-33** confirmed the absence of direct Sb–Sb or O–O bonds, as the interatomic distances were too long to support such bonding interactions (Fig. 16a). The antimony(v) corrole complex, **(Cor)$_2$Sb$_2$^{V}-33**, exhibited excellent electrocatalytic activity for the hydrogen evolution reaction (HER) in dimethylformamide (DMF), using trifluoroacetic acid (TFA) as the proton source. The complex showed a pronounced current enhancement, reaching ∼10 µA at −1.25 V (Fig. 16b and c), indicative of efficient proton reduction facilitated by the reduced form of **(Cor)$_2$Sb$_2$^{V}-33**. Charge accumulation during hydrogen generation was monitored over a 120 s interval and displayed in the corresponding charge *vs.* time plot (Fig. 16d).

Remarkably, a linear increase in charge was observed for more than 21 hours under conditions of 70 mM TFA, demonstrating the long-term electrochemical stability of the catalyst. The **(Cor)$_2$Sb$_2$^{V}-33** complex achieved a faradaic efficiency of ∼80.96%, a TOF of 0.44 h^{-1}, and a hydrogen generation rate of 52.83 µL h^{-1}, confirming its effective performance as a HER catalyst. The term 'faradaic efficiency' refers to how effectively the electrons (or charge) transferred in an electrochemical reaction contribute to the formation of the desired product. The evolution of H$_2$ was further validated by gas chromatography, which confirmed the generation of 158.48 µL of hydrogen over a 3-hour period, corresponding to a consistent production rate of 52.83 µL h^{-1}.[94] During the electrocatalytic hydrogen evolution process, the dimeric complex **(Cor)$_2$Sb$_2$^{V}-33** undergoes *in situ* reduction to form the corresponding antimony(iii) corrole complex, which acts as the true active species for proton reduction. Previous studies have conclusively demonstrated that antimony(iii) corroles serve as the primary electrocatalysts

for H$_2$ evolution, as supported by both experimental data and theoretical calculations.[93,94]

Recently, Liu *et al.* synthesized a series of antimony(iii) corroles structurally analogous to **(Cor)Sb^{III}-1** and the previously reported **(Cor)Sb^{III}-4**, and employed them for electrocatalytic hydrogen evolution in both organic and aqueous media.[95] Their findings highlight that structural modifications of the corrole ring have a profound influence on HER activity. Upon comparing the HER efficiency of antimony(iii)-corrole complexes with other main-group corrole complexes, it was found that phosphorus(v)-corrole[96] and tin(v)-corrole[97] exhibited exceptional catalytic performance, with TOF values of 8.40 h^{-1} and 474.3 h^{-1}, respectively in acetonitrile/water (v/v = 2:3) using water as the proton source. The reported TOF values indicate that phosphorus(v)- and tin(v)-corrole complexes exhibit significantly higher catalytic efficiency compared to antimony(iii)-corroles. While the HER catalyzed by transition and noble metal-based corrole complexes has always received significant attention due to their high TOF and excellent stability.[98] In contrast, most reported antimony(iii)-corrole complexes have demonstrated short-term stability during electrocatalysis, maintaining performance over durations ranging from 4 to 21 hours.[92–94] However, their long-term durability under different practical operational conditions—such as exposure to light, elevated temperatures, and oxidative environments—remains insufficiently explored and warrants further investigation.

Given the significance of hydrogen as a sustainable and clean energy carrier, the development of efficient electrocatalysts for its production has attracted growing interest. While metal complexes, particularly those based on main-group
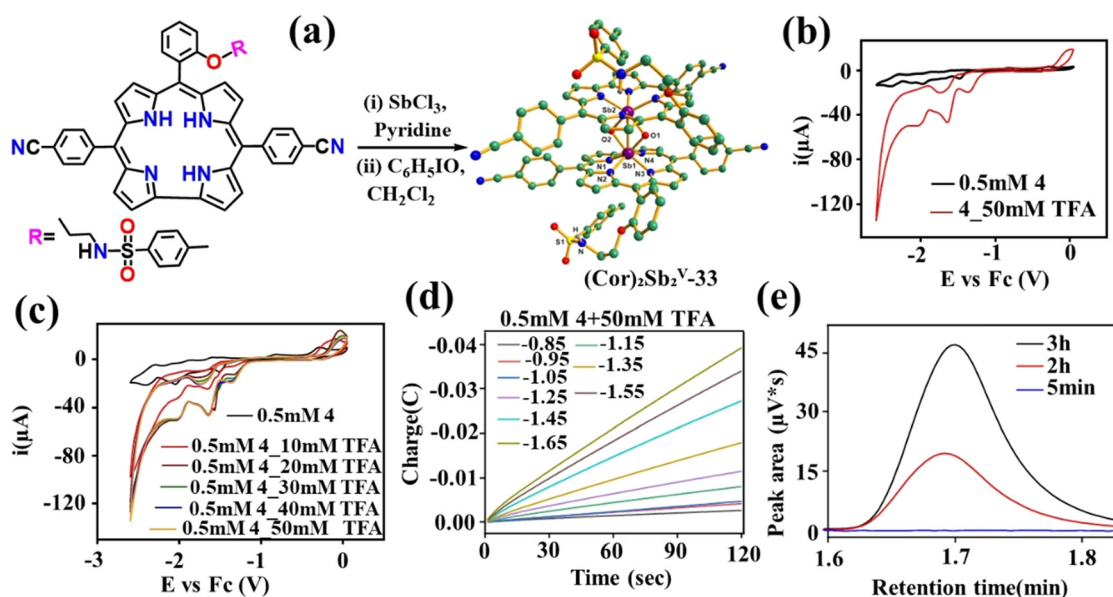
Fig. 16 (a) Molecular structure of FB corrole and the **(Cor)$_2$Sb$_2$^{V}-33** complex, (b) voltammograms of **(Cor)$_2$Sb$_2$^{V}-33** (0.5 mM) in the absence of TFA (black) and under 50 mM TFA (red) recorded under a scan rate of 0.1 V s^{-1}; (c) CV of 0.5 mM **(Cor)$_2$Sb$_2$^{V}-33** with varying amounts of TFA; (d) CPE of 0.5 mM **(Cor)$_2$Sb$_2$^{V}-33** at various applied potentials (v) and (d) gas chromatography (GC) chromatograms of H$_2$ from electrocatalysis of **(Cor)$_2$Sb$_2$^{V}-33**. Adapted from ref. 94 with permission from the American Chemical Society. © 2024 American Chemical Society.

elements, have shown notable promise in HER catalysis, antimony(III/V) corroles represent a relatively under explored yet highly promising class of electrocatalysts. Further rational design and structural tuning of the corrole framework could lead to the development of more robust and efficient HER catalysts based on antimony corroles.

5. Antimony(III/V)-corrole complexes as dielectric and optoelectronic materials

The development of next-generation semiconductors through inorganic technologies has garnered significant attention, particularly in response to the demands of a rapidly growing global population.[99] In contrast, many organic semiconductors are becoming less favorable due to their inherently low dielectric constants (ε_r), typically ranging from 3 to 5.[100] However, certain organic semiconductors incorporating porphyrinoids as donor units demonstrate enhanced thermal and photostability, along with efficient light-harvesting capabilities across a broad range of the solar emission spectrum.[101] Among various porphyrinoids, corroles have emerged as particularly promising candidates for solar energy conversion and optoelectronic applications.[102] Notably, metallocorroles have been extensively utilized in phosphorescent organic light-emitting devices (OLEDs) due to their long triplet-excited-state lifetimes and high emission quantum yields.[103] In addition, metallocorroles exhibit broad absorption bands in the visible region, extending close to 800 nm, thereby significantly enhancing the performance of organic photovoltaic (OPV) devices.[104] Corrole, a

tetrapyrrolic macrocyclic ligand, offers vast opportunities for structural modification, while metalation provides an additional avenue for fine-tuning its optical and chemical properties. Our group is actively working on corroles and metallocorroles, aiming to modify their optical and electronic characteristics to achieve enhanced functionality. Recently, we synthesized and investigated the impact of molecular engineering on the dielectric and optoelectronic properties of antimony corroles, comparing four novel complexes with varying oxidation states and corrole environments.[105] These compounds include: 10-(4-bromophenyl)-5,15-bis(4-cyanophenyl)corrolato}antimony(III){(Cor)Sb^{III}-34}, {2,3,17,18-tetra(thiocyano)-10-(4-bromophenyl)-5,15-bis(4-cyanophenyl)corrolato}antimony(III) {(Cor)Sb^{III}-35}, {10-(4-bromophenyl)-5,15-bis(4-cyanophenyl)corrolato}trans-difluoro antimony(V) {(Cor)Sb^{V}-34a}, and {2,3,17,18-tetra(thiocyano)-10-(4-bromophenyl)-5,15-bis(4-cyanophenyl)corrolato}trans-difluoro antimony(V) {(Cor)Sb^{V}-35a} (Fig. 17a). Dielectric measurements of these antimony(III/V) corrole complexes revealed that substitution at the β-positions of the corrole moiety (SCN or H) significantly influences their dielectric properties. SCN substitution in the antimony(III) complex, (Cor)Sb^{III}-35, increased the ε_r value from 2.5 to 7.2 at f = 1 kHz. In contrast, replacing SCN with H in the antimony(V) complex, (Cor)Sb^{V}-34a, led to a reduction in ε_r from 8.1 to 5.1 at the same frequency (Fig. 17b). These findings underscore the crucial role of SCN substitution in enhancing the dielectric constant ($\varepsilon_r \approx 7$–8), while H substitution yields lower ε_r values, thereby highlighting the significance of targeted structural modifications in optimizing the dielectric properties of antimony corroles.

In solar cell device fabrication, devices incorporating the SCN-substituted antimony(III) corrole [(Cor)Sb^{III}-35] and
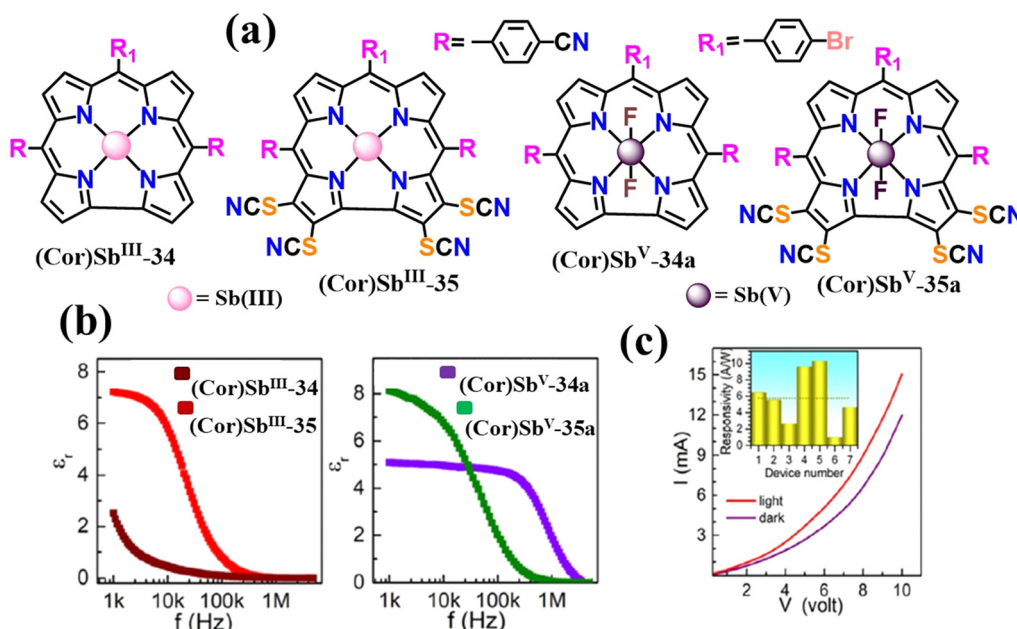
Fig. 17 (a) Molecular structure of antimony(III/V)-corrole complexes; (Cor)Sb^{III}-34, (Cor)Sb^{III}-35, (Cor)Sb^{V}-34a and (Cor)Sb^{V}-35a, (b) impedance measurement plot of four antimony(III/V)-corrole complexes and (c) photoresponse of a hole-only device of antimony(V) corrole (Cor)Sb^{V}-35a. Inset: White light photoresponsivity values of different devices (the dotted line represents the average value). Adapted from ref. 105 with permission from John Wiley and Sons. © 2025 Wiley-VCH.

antimony(v) corrole [**(Cor)Sb^V-35a**] consistently demonstrated an open-circuit voltage (V_{OC}) of approximately 0.7 V. In contrast, devices based on the non-substituted analogues [**(Cor)Sb^{III}-34**] and [**(Cor)Sb^V-34a**] exhibited no significant V_{OC}, indicating that SCN substitution plays a crucial role in enabling high V_{OC} values. When compared to commercial semiconducting molecules such as P3HT and PC61BM, the V_{OC} of the SCN-substituted corroles reached up to 0.72 V, at least three times higher than that of P3HT/PC61BM-based single-component photovoltaic devices. The antimony(v) corrole [**(Cor)Sb^V-35a**], which features broad absorption in the visible region, a high dielectric constant (ε_r), and high charge carrier mobility (μ), was further employed in the fabrication of a single-component photodetector device.[105] The performance data clearly establish the positioning of antimony–corrole complexes—particularly [**(Cor)Sb^V-35a**]—relative to existing commercial and research-grade semiconductors. Most commercial photodetectors, such as silicon-based devices, exhibit photoresponsivities in the range of 100–500 mA W^{-1} at approximately 770 nm.[106] In contrast, devices incorporating the antimony(v) corrole, [**(Cor)Sb^V-35a**], demonstrate average photoresponsivities of $\sim$5.7 A W^{-1}, with peak values reaching 10 A W^{-1} under 0.1 Sun white light illumination (Fig. 17c). These values exceed those of silicon photodetectors by more than an order of magnitude, placing [**(Cor)Sb^V-35a**] among the highest-performing organic photodetectors reported to date. In photovoltaic applications, single-component solar cells based on [**(Cor)Sb^V-35a**] deliver open-circuit voltages (V_{OC}) up to $\sim$0.72 V, which is at least three times higher than the values typically observed in standard P3HT/PCBM systems ($\sim$0.2 V). This enhanced V_{OC} is attributed to the presence of the SCN substituent and the higher oxidation state of antimony (Sb(v)), both of which contribute to deeper HOMO energy levels and improved quasi-Fermi level splitting. Additionally, the high dielectric constant of the corrole macrocycle further facilitates efficient charge separation. Collectively, these metrics demonstrate that antimony–corrole complexes—particularly [**(Cor)Sb^V-35a**]—not only outperform many conventional organic semiconductors in terms of photoresponsivity and photovoltage but also rival or surpass commercial inorganic photodetectors under comparable conditions. These results demonstrate that the enhancement of dielectric and optoelectronic properties through targeted molecular modification of antimony corroles can lead to highly efficient organic electronic materials. This work is expected to inspire further research into macrocyclic frameworks for the development of advanced dielectric and optoelectronic devices.

7. Conclusion and future perspective

This review provides a comprehensive examination of antimony(iii/v)-corrole complexes, highlighting their distinctive structural and electronic features as well as their broad potential applications across various scientific fields. It aims to inspire researchers to develop novel Sb–corrole-based

materials for advanced applications. However, a critical consideration in the development of metallocorrole-based systems remains their thermal and photochemical stability. Although, the trianionic ligand framework of corroles offers excellent stabilization of high-valent metal centers, including Sb(v), their long-term durability under operational conditions—such as light, heat, and oxidative environments—remains insufficiently explored. In photocatalytic or oxidative systems, antimony corroles are particularly vulnerable to demetallation, macrocycle degradation, and axial ligand dissociation. From both thermodynamic and kinetic perspectives, a metal complex is deemed stable when it resists decomposition across a broad range of conditions and when decomposition pathways are hindered by high activation barriers. Strategies to enhance stability should therefore focus on macrocyclic modifications—such as the incorporation of sterically bulky or electron-withdrawing substituents at the *meso*-position—as well as axial ligand engineering to mitigate degradation and enhance resistance to hydrolytic or photolytic breakdown.

Equally important is the issue of scalability. Despite the extensive academic interest in metallocorroles, including antimony derivatives, their translation into practical catalytic or device applications is limited by synthetic protocols that are typically low-yielding, multi-step, and highly sensitive to moisture and oxygen. As emphasized by Ganley and co-workers,[107] translationally relevant organometallic systems must support reproducible, scalable synthesis with minimal operational complexity. Current Sb corrole syntheses often rely on air- and moisture-sensitive reagents such as SbCl$_3$ in pyridine and frequently require glovebox techniques, significantly constraining synthetic throughput. To enable broader adoption, future methodologies must prioritize modular, scalable protocols that employ air-stable reagents, environmentally benign solvents, and conditions compatible with parallel or high-throughput synthesis.[108]

Furthermore, the integration of Sb corroles into solid-state platforms remains a significant challenge. Although these complexes exhibit favorable optical and redox properties in solution, their deployment in functional devices—such as photoelectrodes, redox flow batteries, or organic light-emitting diodes (OLEDs)—necessitates compatibility with processing techniques like spin-coating, inkjet printing, or drop-casting.[109] Embedding Sb corroles into polymer matrices, porous scaffolds (*e.g.*, metal–organic or covalent organic frameworks), or electroactive films will be essential to achieve operational robustness and device-level performance. Hybridization strategies, including covalent grafting, axial ligand tuning, and surface anchoring onto conductive or semiconducting supports (*e.g.*, TiO$_2$, g-C$_3$N$_4$), offer promising routes to enhance photostability, promote charge separation, and expand functionality in photoelectrochemical cells and solar fuel generation.[110–113] However, these approaches remain underdeveloped for antimony corroles and represent a fertile area for future research.

Author contributions

Writing – review and editing: AT, TP, SK, RC, and SK; funding acquisition and manuscript revision: AT and SK; all authors have read and approved the final manuscript.

Conflicts of interest

The authors declare no competing financial interest.

Data availability

This review does not include any primary research results, software, or code. No new data were generated or analyzed as part of this work.

Acknowledgements

References

1 Z. Gross, G. Golubkov and L. Simkhovich, *Angew. Chem., Int. Ed.*, 2000, **39**, 4045–4047.
2 S. Hiroto, Y. Miyake and H. Shinokubo, *Chem. Rev.*, 2017, **117**, 2910–3043.
3 C. C. Wamser and A. Ghosh, *JACS Au*, 2022, **2**, 1543–1560.
4 Q. Sun, L. M. Mateo, R. Robles, P. Ruffieux, N. Lorente, G. Bottari, T. Torres and R. Fasel, *J. Am. Chem. Soc.*, 2020, **142**, 18109–18117.
5 A. Kumar, D. Kim, S. Kumar, A. Mahammed, D. G. Churchill and Z. Gross, *Chem. Soc. Rev.*, 2023, **52**, 573–600.
6 T. E. Shubina, H. Marbach, K. Flechtner, A. Kretschmann, N. Jux, F. Buchner, H. P. Steinrück, T. Clark and J. M. Gottfried, *J. Am. Chem. Soc.*, 2007, **129**, 9476–9483.
7 H. Zhu, G. Wen, W. Zheng, N. H. Rees, W. Stawski, H. I. Wang, M. Bonn and H. L. Anderson, *Angew. Chem., Int. Ed.*, 2025, **137**, e202417429.
8 W. Sinha, A. Mahammed, N. Fridman, Y. Diskin-Posner, L. J. Shimon and Z. Gross, *Chem. Commun.*, 2019, **55**, 11912–11915.
9 I. Yadav, V. Prakash, M. R. Maurya and M. Sankar, *Inorg. Chem.*, 2023, **62**, 5292–5301.
10 A. Kumar, P. Yadav, M. Majdoub, I. Saltsman, N. Fridman, S. Kumar, A. Kumar, A. Mahammed and Z. Gross, *Angew. Chem., Int. Ed.*, 2021, **133**, 25301–25307.
11 A. Johnson and I. Kay, *J. Chem. Soc.*, 1965, 1620–1629.
12 D. Nurco and K. Smith, *Chem. Commun.*, 1999, 1307–1308.
13 A. B. Alemayehu, K. E. Thomas, R. F. Einrem and A. Ghosh, *ACS Cent. Sci.*, 2021, **54**, 3095–3107.
14 S. Nardis, F. Mandoj, M. Stefanelli and R. Paolesse, *Coord. Chem. Rev.*, 2019, **388**, 360–405.
15 R. Padilla, H. L. Buckley, A. L. Ward and J. Arnold, *Chem. Commun.*, 2014, **50**, 2922–2924.
16 W. Lee, X. Zhan, J. Palma, J. Vestfrid, Z. Gross and D. G. Churchill, *Chem. Commun.*, 2021, **57**, 4605–4641.
17 I. Saltsman, I. Goldberg and Z. Gross, *Org. Lett.*, 2015, **17**, 3214–3217.
18 N. Holzer, J. Jin, V. N. Nesterov, J. K. Sharma, N. Zarrabi, F. D'Souza and P. K. Poddutoori, *Inorg. Chem.*, 2023, **62**, 7097–7110.
19 K. M. Kadish, C. Erben, Z. Ou, V. A. Adamian, S. Will and E. Vogel, *Inorg. Chem.*, 2000, **39**, 3312–3319.
20 V. A. Vaillard, P. D. Nieres, S. E. Vaillard, F. Doctorovich, B. Sarkar and N. I. Neuman, *Eur. J. Inorg. Chem.*, 2022, e202100767.
21 B. Basumatary, R. V. R. Reddy, S. Bhandary and J. Sankar, *Dalton Trans.*, 2015, **44**, 20817–20821.
22 L. Yun, H. V.- Lima, H. Fang, Z. Yao, G. Geisberger, C. Dietl, A. Ghosh, P. J. Brothers and X. Fu, *Inorg. Chem.*, 2014, **53**, 7047–7054.
23 L. M. Reith, M. Stiftinger, U. Monkowius, G. Knör and W. Schoefberger, *Inorg. Chem.*, 2011, **50**, 6788–6797.
24 A. M. Tedy and A. K. Manna, *Phys. Chem. Chem. Phys.*, 2024, **26**, 27466–27477.
25 A. Mahammed, H. B. Gray and Z. Gross, *Chem. Rev.*, 2025, **125**, 2809–2845.
26 K. M. Kadish, Z. Ou, V. A. Adamian, R. Guilard, C. P. Gros, C. Erben, S. Will and E. Vogel, *Inorg. Chem.*, 2000, **39**, 5675–5682.
27 I. Yadav, D. Dhiman and M. Sankar, *Chem. Commun.*, 2024, **60**, 13456–13467.
28 A. Tarai, J. Mallick, P. Singh, J. Conradie, S. Kar and A. Ghosh, *J. Org. Chem.*, 2023, **88**, 13022–13029.
29 P. Yadav and M. Sankar, *Dalton Trans.*, 2014, **43**, 14680–14688.
30 C. I. M. Santos, E. Oliveira, J. F. B. Barata, M. A. F. Faustino, J. A. S. Cavaleiro, M. G. P. M. S. Neves and C. Lodeiro, *J. Mater. Chem.*, 2012, **22**, 13811–13819.
31 I. Luobeznova, M. Raizman, I. Goldberg and Z. Gross, *Inorg. Chem.*, 2006, **45**, 386–394.
32 L. Wagnert, A. Berg, E. Stavitski, I. Luobeznova, Z. Gross and H. Levanon, *J. Porphyrins phthalocyanines*, 2007, **11**, 645–651.
33 C. Zahn, T. Stensitzki, M. Gerecke, A. Berg, A. Mahammed, Z. Gross and K. Heyne, *Molecules*, 2017, **22**, 1174.
34 S. Mondal, A. Garai, P. K. Naik, J. K. Adha and S. Kar, *Inorg. Chim. Acta*, 2020, **501**, 119300.
35 C. M. Lemon, A. G. Maher, A. R. Mazzotti, D. C. Powers, M. I. Gonzalez and D. G. Nocera, *Chem. Commun.*, 2020, **56**, 5247–5250.
36 S. Mondal, T. Pain, M. Villa, S. Angeloni, A. Tarai, P. Ceroni and S. Kar, *Eur. J. Inorg. Chem.*, 2023, e202300283.
37 V. Caliskanyürek, S. Eulberg, O. Lange, M. Bröring and S. Tschierlei, *Chem. Commun.*, 2024, **60**, 4096–4099.
38 C. M. Lemon, S. J. Hwang, A. G. Maher, D. C. Powers and D. G. Nocera, *Inorg. Chem.*, 2018, **57**, 5333–5342.
39 H. C. Honig, A. Friedman, N. Zion and L. Elbaz, *Chem. Commun.*, 2020, **56**, 8627–8630.
40 P. Yadav, S. Khoury, A. Mahammed, M. Morales, S. C. Virgil, H. B. Gray and Z. Gross, *Org. Lett.*, 2020, **22**, 3119–3122.
41 A. Mahammed and Z. Gross, *J. Am. Chem. Soc.*, 2023, **145**, 12429–12445.
42 W. Sinha, M. G. Sommer, N. Deibel, F. Ehret, M. Bauer, B. Sarkar and S. Kar, *Angew. Chem., Int. Ed.*, 2015, **54**, 13769–13774.
43 S. Eulberg, N. Schulze, J. Krumsieck, N. Klein and M. Bröring, *Angew. Chem., Int. Ed.*, 2023, **62**, e202306598.
44 R. F. Epping, F. J. de Zwart, N. P. van Leest, J. I. van der Vlugt, M. A. Siegler, S. Mathew, J. N. Reek and B. de Bruin, *Inorg. Chem.*, 2024, **63**, 1974–1987.
45 D. J. Kim, K. R. Hermann, A. Prokofjevs, M. T. Otley, C. Pezzato, M. Owczarek and J. F. Stoddart, *J. Am. Chem. Soc.*, 2017, **139**, 6635–6643.
46 X. Su, K. M. McCardle, J. A. Panetier and J. W. Jurss, *Chem. Commun.*, 2018, **54**, 3351–3354.
47 N. Pradhan, A. Garai, B. Patra, S. Kar and P. K. Maiti, *Chem. Commun.*, 2021, **57**, 4851–4854.
48 A. B. Alemayehu, K. E. Thomas, R. F. Einrem and A. Ghosh, *Acc. Chem. Res.*, 2021, **54**, 3095–3107.
49 A. Mahammed, K. Chen, J. Vestfrid, J. Zhao and Z. Gross, *Chem. Sci.*, 2019, **10**, 7091–7103.
50 C. D. Natale, C. P. Gros and R. Paolesse, *Chem. Soc. Rev.*, 2022, **51**, 1277.
51 A. Mahammed and Z. Gross, *Angew. Chem., Int. Ed.*, 2015, **127**, 12547–12550.
52 S. Mondal, T. Pain, A. Mandal, D. Maiti and S. Kar, *Appl. Organomet. Chem.*, 2023, **37**, e7088.
53 J. F. Barata, M. G. P. Neves, M. A. F. Faustino, A. C. Tome and J. A. Cavaleiro, *Chem. Rev.*, 2017, **117**, 3192–3253.
54 A. P. Ghosh, P. Lodowski, A. Bazarganpour, M. Leks and P. M. Kozlowski, *Dalton Trans.*, 2020, **49**, 4114–4124.
55 S. Jockusch and B. Kräutler, *Chem. Commun.*, 2025, **61**, 3904–3907.
56 S. Han, Y. Liu, D. Peng, J. Liu and D. Wu, *Bioconjug. Chem.*, 2023, **34**, 2155–2180.
57 I. Aviv and Z. Gross, *Chem. Commun.*, 2007, 1987–1999.
58 A. Mahammed and Z. Gross, *Coord. Chem. Rev.*, 2019, **379**, 121–132.
59 Z. Zhang, H. H. Wang, H. J. Yu, Y. Z. Xiong, H. T. Zhang, L. N. Ji and H. Y. Liu, *Dalton Trans.*, 2017, **46**, 9481–9490.

60 R. F. Einrem, A. B. Alemayehu, S. M. Borisov, A. Ghosh and O. A. Gederaas, *ACS Omega*, 2020, **5**, 10596–10601.

61 M. Soll, V. K. Sharma, S. Khoury, Y. G. Assaraf and Z. Gross, *J. Med. Chem.*, 2022, **66**, 766–776.

62 V. K. Sharma, M. Stark, N. Fridman, Y. G. Assaraf and Z. Gross, *J. Med. Chem.*, 2022, **65**, 6100–6115.

63 K. Sahu, S. Angeloni, J. Conradie, M. Villa, M. Nayak, A. Ghosh, P. Ceroni and S. Kar, *Dalton Trans.*, 2022, **51**, 13236.

64 A. Preuß, I. Saltsman, A. Mahammed, M. Pfitzner, I. Goldberg, Z. Gross and B. Röder, *J. Photochem. Photobiol., B*, 2014, **133**, 39–46.

65 X. Liang, J. Mack, L. M. Zheng, Z. Shen and N. Kobayashi, *Inorg. Chem.*, 2014, **53**, 2797–2802.

66 H. Agadjanian, J. Ma, A. Rentsendorj, V. Valluripalli, J. Y. Hwang, A. Mahammed, D. L. Farkas, H. B. Gray, Z. Gross and L. K. Medina-Kauwe, *Proc. Natl. Acad. Sci. U. S. A.*, 2009, **106**, 6105–6110.

67 Z. H. Liang, H. Y. Liu, R. Zhou, Z. Zhang, A. Ali, B. J. Han, Y. J. Liu and X. Y. Xiao, *J. Membr. Biol.*, 2016, **249**, 419–428.

68 F. Cheng, H. H. Wang, A. Ali, J. Kandhadi, H. Wang, X. L. Wang and H. Y. Liu, *J. Porphyrins phthalocyanines*, 2018, **22**, 886–898.

69 Y. G. Wang, Z. Zhang, H. Wang and H. Y. Liu, *Bioorg. Chem.*, 2016, **67**, 57–63.

70 A. N. Xie, Z. Zhang, H. H. Wang, A. Ali, D. X. Zhang, H. Wang, L. N. Ji and H. Y. Liu, *J. Porphyrins phthalocyanines*, 2018, **22**, 739–750.

71 D. E. Fitzpatrick, C. Battilocchio and S. V. Ley, *ACS Cent. Sci.*, 2016, **2**, 131–138.

72 T. Dalton, T. Faber and F. Glorius, *ACS Cent. Sci.*, 2021, **7**, 245–261.

73 J. H. Docherty, T. M. Lister, G. Mcarthur, M. T. Findlay, P. Domingo-Legarda, J. Kenyon, S. Choudhary and I. Larrosa, *Chem. Rev.*, 2023, **123**, 7692–7760.

74 A. E. Shilov and G. B. Shul'pin, *Chem. Rev.*, 1997, **97**, 2879–2932.

75 J. Takaya, *Chem. Sci.*, 2021, **12**, 1964–1981.

76 H. Lu and X. P. Zhang, *Chem. Soc. Rev.*, 2011, **40**, 1899–1909.

77 R. Singh and A. Mukherjee, *ACS Catal.*, 2019, **9**, 3604–3617.

78 W. C. C. Lee, J. Wang, Y. Zhu and X. P. Zhang, *J. Am. Chem. Soc.*, 2023, **145**, 11622–11632.

79 M. Mahajan and B. Mondal, *JACS Au*, 2023, **3**, 3494–3505.

80 M. Mahajan and B. Mondal, *Inorg. Chem.*, 2023, **62**, 5810–5821.

81 Z. Wang, J. Cheng, W. Ding and D. Wang, *Organometallics*, 2022, **41**, 569–580.

82 T. Pain, A. K. Singh, A. Tarai, S. Mondal, A. Indra and S. Kar, *Inorg. Chem.*, 2023, **62**, 18779–18788.

83 L. Schlapbach and A. Züttel, *Nature*, 2001, **414**, 353–358.

84 G. Di Liberto, L. A. Cipriano and G. Pacchioni, *J. Am. Chem. Soc.*, 2021, **143**, 20431–20441.

85 F. Zaera, *Energy Fuels*, 2025, **39**, 2422–2434.

86 M. Li, K. Duanmu, C. Wan, T. Cheng, L. Zhang, S. Dai, W. Chen, Z. Zhao, P. Li, H. Fei, Y. Zhu, R. Yu, J. Luo, K. Zang, Z. Lin, M. Ding, J. Huang, H. Sun, J. Guo, X. Pan, W. A. Goddard, P. Sautet, Y. Huang and X. Duan, *Nat. Catal.*, 2019, **2**, 495–503.

87 W. Li, X. Peng, H. Qin, Y. Xu, J. Han, H. Lei and R. Cao, *Dalton Trans.*, 2024, **53**, 19121–19125.

88 G. Yang, Z. Ullah, W. Yang, H. Wook Kwon, Z. X. Liang, X. Zhan, G. Q. Yuan and H. Y. Liu, *ChemSusChem*, 2023, **16**, e202300211.

89 J. Jiang, K. L. Materna, S. Hedström, K. R. Yang, R. H. Crabtree, V. S. Batista and G. W. Brudvig, *Angew. Chem., Int. Ed.*, 2017, **56**, 9111–9115.

90 N. Wang, H. Lei, Z. Zhang, J. Li, W. Zhang and R. Cao, *Chem. Sci.*, 2019, **10**, 2308–2314.

91 H. Lei, X. Li, J. Meng, H. Zheng, W. Zhang and R. Cao, *ACS Catal.*, 2019, **9**, 4320–4344.

92 Q. W. Yan, L.-W. Wu, Z. W. Liu, F. Chen, C. Ling, H. Y. Liu, X. Y. Xiao and L. P. Si, *Green Chem.*, 2024, **26**, 4574–4581.

93 S. Kumar, S. Fite, E. Remigi, A. Mizrahi, N. Fridman, A. Mahammed, T. P. Bender and Z. Gross, *Chem. - Eur. J.*, 2024, **30**, e202402145.

94 R. Chakraborty, B. Ojha, T. Pain, T. W. Tsega, A. Tarai, N. C. Jana, C.-H. Hung and S. Kar, *Inorg. Chem.*, 2024, **63**, 21462–21473.

95 Q. H. Yu, Y. F. Li, X. Y. Cao, L. H. Liu, J. Chen, L. P. Si and H. Y. Liu, *Dalton Trans.*, 2025, **54**, 4935–4940.

96 G. Yang, Z. Ullah, W. Yang, H. W. Kwon, Z. X. Liang, X. Zhan, G. Q. Yuan and H. Y. Liu, *ChemSusChem*, 2023, **16**, e202300211.

97 B. P. Ren, G. Yang, Z. Y. Lv, Z. Y. Liu, H. Zhang, L. P. Si and H. Y. Liu, *Inorg. Chem. Commun.*, 2023, **152**, 110663.

98 H. Lei, H. Fang, Y. Han, W. Lai, X. Fu and R. Cao, *ACS Catal.*, 2015, **5**, 5145–5153.

99 H. Yao and J. Hou, *Angew. Chem., Int. Ed.*, 2022, **61**, e202209021.

100 S. Chen, S. W. Tsang, T. H. Lai, J. R. Reynolds and F. So, *Adv. Mater.*, 2014, **26**, 6125.

101 M. Urbani, G. de la Torre, M. K. Nazeeruddin and T. Torres, *Chem. Soc. Rev.*, 2019, **48**, 2738.

102 T. Higashino, Y. Kurumisawa, A. B. Alemayehu, R. F. Einrem, D. Sahu, D. Packwood, K. Kato, A. Yamakata, A. Ghosh and H. Imahori, *ACS Appl. Energy Mater.*, 2020, **3**, 12460.

103 S. L. Lai, W. Y. Tong, S. C. Kui, M. Y. Chan, C. C. Kwok and C. M. Che, *Adv. Funct. Mater.*, 2013, **23**, 5168.

104 A. Agresti, B. Berionni Berna, S. Pescetelli, A. Catini, F. Menchini, C. Di Natale, R. Paolesse and A. Di Carlo, *Adv. Funct. Mater.*, 2020, **30**, 2003790.

105 T. Pain, Md Saifuddin, A. Sahoo, B. Mahapatra, S. Kar, R. Chakraborty, S. P. Senanayak and S. Kar, *Small Sci.*, 2025, 2400589.

106 M. Yang, K. Rim, D. L. Rogers, J. D. Schaub, J. J. Welser, D. M. Kuchta, D. C. Boyd, F. Rodier, P. A. Rabidoux, J. T. Marsh, A. D. Ticknor, Q. Yang, A. Upham and S. C. Ramac, *IEEE Electron Dev. Lett.*, 2002, **23**, 395–397.

107 J. M. Ganley, C. L. Joe and E. M. Simmons, *ACS Catal.*, 2025, **15**, 8317–8336.

108 J. Götz, M. K. Jackl, C. Jindakun, A. N. Marziale, J. André, D. J. Gosling, C. Springer, M. Palmieri, M. Reck and A. Luneau, *Sci. Adv.*, 2023, **9**, eadj2314.

109 C. S. Buga and J. C. Viana, *Adv. Mater. Technol.*, 2021, **6**, 2001016.

110 G. Z. S. Ling, S. F. Ng and W. J. Ong, *Adv. Funct. Mater.*, 2022, **32**, 2111875.

111 A. Hayat, M. Sohail, A. El Jery, K. M. Al-Zaydi, K. F. Alshammari, J. Khan, H. Ali, Z. Ajmal, T. Taha and I. Ud Din, *Chem. Rec.*, 2023, **23**, e202200171.

112 W.-J. Ong, L.-L. Tan, Y. H. Ng, S.-T. Yong and S.-P. Chai, *Chem. Rev.*, 2016, **116**, 7159–7329.

113 Y. Wang, S. Zhong, Z. Niu, Y. Dai and J. Li, *Chem. Commun.*, 2023, **59**, 10883–10911.